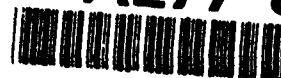


Typhoon Monitoring Using Passive Satellite Observations

A Final Report on DoD Contract N00014-88-K-0711

A REPORT from the

AD-A277 859



METEOROLOGICAL

SATELLITE

STUDIES

DTIC

SELECTE

APR 7 1994

Permittances

Typhoon Monitoring Using Passive Satellite Observations

A Final Report on DoD Contract N00014-88-K-0711

for the period 1 April 1988 though 31 December 1993


Prepared by Christopher Velden and Robert Merrill (Co-Principal Investigators)

on behalf of

The Cooperative Institute for Meteorological Satellite Studies
Space Science and Engineering Center (SSEC)
at the University of Wisconsin-Madison
1225 West Dayton Street
Madison, Wisconsin 53706
608 262-9168

Accession For	
NTIS CRA&I	<input checked="" type="checkbox"/>
DTIC TAB	<input type="checkbox"/>
Unannounced	<input type="checkbox"/>
Distribution /	
Availability Codes	
Dist	Avail and/or Special
A-1	

Sept 94-06450



February 1994

DTIC QUALITY INSPECTED 2

94 2 25 174

April 1988 through December 1993 Activity under DoD Contract N00014-88-K-0711

SUMMARY OF SCIENTIFIC GOALS

During the 5 1/2 years that this contract was active, the scientific goals evolved to include three main areas of research: 1) Typhoon monitoring using passive microwave observations, 2) The ONR tropical cyclone motion initiative, and 3) Participation in the tropical cyclone motion field experiment (TCM-90). Accomplishments and scientific results from each of these topics are summarized below, with details given in the Appendices.

FINANCIAL SUMMARY

A total of \$290,369 was provided to support the tasks of this contract. Spending terminated on 31 December, 1993. Of the total spent, \$121,988 was used to support the research on microwave applications, and \$168,381 went to support the motion experiment and related research.

SUMMARY OF ACCOMPLISHMENTS AND SCIENTIFIC RESULTS

1) Typhoon Monitoring Using Passive Microwave Observations

Funding (\$121,988) from the Air Force Geophysics Laboratory (now Phillips Laboratory) administered through N00014-88-K-0711 supported the development of techniques to estimate the intensities of typhoons from satellites. Specifically, our objectives were to develop practical techniques for estimating tropical cyclone intensities from the current generation of microwave radiometers, the Microwave Sounding Unit (MSU) on board the civilian NOAA series spacecraft, and the Special Sensor, Microwave/Temperature (SSM/T) on the Defense Meteorological Satellite Program (DMSP) spacecraft. The physical basis of these techniques lies in the structure of tropical cyclones and the properties of microwave radiation in the 55 GHz band. The maximum wind speeds of typhoons are closely related to the reduction in sea level pressure at the center, which is in turn directly related to the magnitude of the warming in the upper-troposphere (roughly 150-500 hPa). At terrestrial temperatures, molecular oxygen (O₂) emits small quantities of microwave radiation at frequencies around 55 GHz (wavelength of 0.5 cm). The quantity emitted is proportional to the air temperature so the strength of the tropical cyclone warm anomaly can be deduced from the amount of microwave radiation coming from the storm center relative to the surroundings. The stronger the radiation from the center, the stronger the warm core and therefore the pressure drop and surface winds. This is also true of radiation at higher frequencies (such as infrared), but microwaves are uniquely suited to tropical cyclones because they alone can pass largely unattenuated through accompanying thick cirrus cloud canopies.

a. statistical technique

The first technique developed involved a statistical relationship between MSU observations and western North Pacific typhoon intensity, and was an extension of an earlier study which examined Atlantic hurricanes. Microwave radiation at four distinct frequencies observed by the MSU was used to prepare atmospheric soundings at the storm center and around its periphery. The strength of the warm anomaly was defined by the retrieved temperatures at 250 hPa (about 11 km altitude), which is the typical level of maximum warming in typhoons. Nonlinear regression relationships were then fitted between these warm anomaly measurements and surface pressure reductions and maximum wind speeds, respectively for 82 western North Pacific tropical cyclones of the period 1980-1984. Figure 2 in Appendix 3 shows the resulting statistical relationships on the dependent data set. Other factors such as eye diameter, latitude, intensity tendency, and climatological intensity distribution were also investigated with the following conclusions:

- 1) Overall on the dependent sample, the technique can estimate the central pressure reduction with a standard error of estimate (SEE) of 13.2 hPa.
- 2) Because the sample used to develop the technique contained a large percentage of intense storms for which the estimates tended to be poorer, it was estimated that the *expected* root-mean-squared (RMS) error of the technique applied to all storms in the western North Pacific would be around 11-12 hPa.
- 3) Intensities of filling storms can be estimated most accurately, with an SEE of 9.5 hPa.
- 4) Estimates of the intensities of deepening storms are less accurate (SEE of 15.1 hPa) and depend upon the eye size, with storms having smaller eyes being more intense.

These results are described in further detail in Velden and Merrill (1990) and Velden *et al.* (1991), which can be found in Appendices 7 and 3, respectively.

b. physical technique

A technique that could also be applied to SSM/T data is desirable, but the direct statistical approach described above was impossible. The statistical relationships already described for MSU cannot be applied directly because the fields of view (FOV) of the two sensors are of different sizes (110 km and 180 km respectively) and both are larger than the 25-75 km diameter of the peak warming of a tropical cyclone. Even under the best of conditions, the microwave observations of the warm anomaly underestimate its actual strength because they are influenced somewhat by the region outside the peak warming. The statistical relationships for MSU contain an implicit correction for that sensor's underestimate but are not appropriate for SSM/T. It was also not possible to develop separate statistical relationships for SSM/T, because doing so requires nearly simultaneous SSM/T observations and aircraft reconnaissance ground truth estimates. However, western North Pacific reconnaissance was discontinued in 1987 and the available SSM/T archive begins in 1988.

The approach chosen was to model explicitly the interaction between the antenna pattern and the position, horizontal size and shape, and amplitude of the warm anomaly. A numerical approximation of this model can then be used within the formalism of maximum likelihood estimation to retrieve the warm anomaly strength from a set of passive microwave observations near and around the storm center. The warm anomaly structure is approximated by a function of radius from the storm center that has four parameters which can be varied; its size, shape, and amplitude, and the background brightness temperature. The following steps are used to estimate the warm anomaly strength:

- 1) Given an initial estimate, or "constraint" of all of the warm anomaly structure parameters, use the model structure and satellite navigation, viewing geometry, and antenna pattern to predict what the observed radiances (brightness temperatures) should be in a particular case.

- 2) Compare the predicted brightness temperatures with the actual observations and adjust the structure parameters so as to make the predicted brightness temperatures agree more closely with the observations.
- 3) Compare the new structure parameters with the constraint values and adjust again to minimize differences where possible
- 4) Repeat 2) and 3) iteratively until the "most likely" values of the structure parameters are obtained, given the constraint values and the observations.

A preliminary version of the technique was refined by adding a linear function of latitude and longitude to the background brightness temperature, and the addition of simulation capability to allow SSM/T antenna patterns and scan geometry to be tested. This later version of the technique was applied to a 77-case subset of Velden et al.'s (1991) western North Pacific sample. This preliminary research proved the concept of the technique by showing that the retrieved warm anomalies were better estimators of tropical cyclone intensity than warm anomalies estimated from raw MSU data before retrieval. Simple simulation studies with an SSM/T antenna pattern (but still using MSU scan geometry) also showed that the technique could correct for the antenna pattern differences (see Appendix 5 for further details).

Based on these results, work began on an operational prototype that would be able to both simulate and process observations from both MSU and SSM/T. The operational prototype also adds warm anomaly position to the retrieved parameters and allows for explicit treatment of the effects of position estimate errors on the results. This work commenced under grant N00014-88-K-0711 and has continued under contract N00014-91-J-4158 which ends on 30 September 1994. Simulations of algorithm performance for both MSU and SSM/T for a variety of scan geometries, warm anomaly amplitudes, sizes, and shapes, and estimated position errors are the subject of a recently submitted manuscript (abstract in Appendix 1).

2) The ONR-Sponsored Tropical Cyclone Motion Initiative

Forecasters have long suspected that the motion of tropical cyclones is primarily governed by the surrounding environmental flow, often referred to as "environmental steering". Recent studies have identified other influences, however it is still accepted that the environmental flow is the dominant mechanism in most cases. Our research objectives under the motion initiative were to define this environmental steering in terms of tropospheric depth, and in relation to storm intensity. This work is based on the hypothesis (and some supporting evidence) that intense (weak) tropical cyclones are generally associated with a greater (shallower) vertical development of the cyclonic vortex wind field. The vortex is in turn advected by an environmental flow determined (in a vertical sense) by the tropospheric depth of the vortex wind field.

To test this hypothesis, track forecast sensitivity experiments were performed using a barotropic forecast model. The model was initialized with environmental wind fields derived using varying tropospheric depths. The resultant track forecasts were then compared to actual tracks (using best track data) in order to determine the layer which best approximated future motion. Once determined, the optimum layer flow field was then compared to the storm intensity to investigate a relationship between steering depth and storm intensity. This procedure was repeated for a large sample of cases. In order to determine if the relationship between steering depth and intensity is a universal one, the study included two independent tropical cyclone basins (Australian and Atlantic). The results of this study will allow the operational community to better assess the current and future steering regimes on a case by case basis, and can also be used to more properly initialize numerical track forecast models that use a layer-mean wind analysis as initial input.

The results of our work show that the motion of Australian region tropical cyclones is best approximated by tropospheric layer-mean wind analyses of variable thickness depending on storm intensity. Barotropic model track forecasts were used to specifically determine the optimum layer of environmental steering for different intensity classes. Selected combinations of horizontal and layer-mean wind analyses were used to initialize the forecast model for 300 cases covering a wide range of intensities. Results of the sensitivity tests indicate that shallow layer-means consistently outperform single-level analyses, and are best correlated with storm motion in weak and moderate intensity cases. Deep layer-means are best correlated with future motion only in very intense cases (see Appendices 4 and 6 for further details).

In the Atlantic basin, a similar approach was utilized to identify the steering/intensity relationship. The general trend observed in the Australian region (increasing depth of layer-mean wind steering with increasing intensity) was also found in the Atlantic. However, the relationships were not identical. In general, Atlantic storms of a given intensity are steered by a layer of greater depth (100 mb) than Australian counterparts. See Appendix 2 for further details.

An important accomplishment arising from this research is the specific identification of a quantitative relationship between the depth of the environmental steering (which controls much of the motion) and the intensity of tropical cyclones in two different basins. This finding confirms the hypothesis that a fixed level, or deep layer-mean flow should not be assumed for all intensity classes to describe the environmental (or basic) flow governing tropical cyclone motion, or to initialize operational and research numerical guidance. Instead, attention should be given to the current storm intensity to determine the tropospheric layer which best approximates steering.

3) *Participation in the 1990 Tropical Cyclone Motion Field Experiment (TCM-90)*

As part of an international initiative to better understand the motion of tropical cyclones, a major field experiment was conducted in the western North Pacific Ocean in August-September of 1990. A task of this contract involved the collection, archival, post-processing and dissemination of satellite data and products in support of the field phase. The archive contained imagery and quantitative observations from GMS, NOAA and DMSP satellites. Deliverables to the project data manager and participants included hard-copy imagery, and a videotape containing animated satellite loops of the full experiment period as well as selected interesting cases.

A major effort involved the post-processing of satellite imagery into quantitative wind information. Despite the increased coverage of upper-tropospheric observations from *in situ* TCM-90 platforms, large data void areas still remained within the experiment domain. In order to help fill some of these voids, wind vector sets derived from sequential satellite imagery were produced at 6-hourly intervals during active tropical cyclone periods. High-density, three-dimensional vector fields were produced covering the TCM-90 domain. These vectors were carefully quality-controlled and assigned heights based on comparison with nearby TCM-90 upper-air observations. Environmental features (such as circulations, outflow jets, troughs/ridges) were better-defined, and the observations were deemed an important contribution to the TCM-90 objective analyses (R. Elsberry-Project Director, and E. Rodgers-NMC, personal communication).

PUBLICATIONS

Merrill, R.T., 1994: Simulations of physical retrieval of tropical cyclone structure using 55 GHz band passive microwave observations from polar-orbiting satellites. Submitted to *J. Appl. Meteor.*

Velden, C.S.: The relationship between tropical cyclone motion, intensity and the vertical extent of the environmental steering layer in the Atlantic basin. *20th Conf. Hurr. and Trop Meteor.*, San Antonio, TX, May, 1993.

Velden, C.S., B.M. Goodman and R.T. Merrill, 1991: Western North Pacific tropical cyclone intensity estimation from NOAA polar-orbiting satellite microwave data. *Mon. Wea. Rev.*, **119**, 159-168.

Velden, C.S., and L.M. Leslie, 1991: The basic relationship between tropical cyclone intensity and the depth of the environmental steering layer in the Australian region. *Wea. and Forecasting* **6**, 244-253.

Merrill, R.T.: Physical retrieval of typhoon structure using passive microwave observations. *19th Conf. Hurr. Trop. Meteor.*, Miami, FL, May, 1991.

Velden, C.S., and L.M. Leslie: The relationship between tropical cyclone intensity and the depth of the environmental steering layer in the Australian region. *19th Conf. Hurr. Trop. Meteor.*, Miami, FL, May, 1991.

Velden, C.S, and R.T. Merrill: Western North Pacific tropical cyclone intensity estimation from NOAA polar-orbiting satellite microwave data. *5th Conf. Sat. Meteor. and Ocean.*, London, England, September, 1990, 426-431.

Velden and Merrill; *Numerous* tropical cyclone workshop reports and contributions.

Appendix 1.

**SIMULATIONS OF PHYSICAL RETRIEVAL OF TROPICAL CYCLONE
STRUCTURE USING 55 GHz BAND PASSIVE MICROWAVE
OBSERVATIONS FROM POLAR-ORBITING SATELLITES**

**Robert T. Merrill
Cooperative Institute for Meteorological
Satellite Studies**

**University of Wisconsin
Madison, WI 53706**

**Submitted to
Journal of Applied Meteorology**

February 1994

Abstract

A method for estimating the horizontal structure of the upper-tropospheric warm anomaly of tropical cyclones from 55 GHz microwave observations is presented. Because the peak warming occurs over an area smaller than that viewed by current and planned satellite antenna systems, it is necessary to model explicitly the interaction of the warm anomaly structure and antenna gain pattern. This forward model is then inverted using a maximum-likelihood algorithm with constraints, analogous to that used for thermodynamic sounding retrieval or optimal interpolation but with the retrieved structure represented as an analytic function with variable coefficients rather than a discrete distribution of atmospheric properties in space. Simulation studies demonstrate the overall soundness of the technique and its possible performance and limitations when applied to two different polar-orbiting microwave sensors, MSU and SSM/T.

Appendix 2.

Presented at the 20th Conf. Hurricanes and Tropical Meteorology,
San Antonio, TX, May 1993.

THE RELATIONSHIP BETWEEN TROPICAL CYCLONE MOTION, INTENSITY AND THE VERTICAL EXTENT OF THE ENVIRONMENTAL STEERING LAYER IN THE ATLANTIC BASIN

Christopher Velden

*University of Wisconsin-Space Science and Engineering Center
Madison, Wisconsin 53706*

1. INTRODUCTION

Forecasters have long suspected that the motion of tropical cyclones is primarily governed by a surrounding environmental flow, sometimes referred to as a "steering current". We have recently learned that this general concept is too simplistic, however it is still commonly accepted that the environmental flow plays a major role. It is therefore important, both for research modeling and operational forecasting purposes, to properly define this three-dimensional environmental flow field.

In this paper, we attempt to quantitatively identify the vertical extent of the optimum tropical cyclone steering layer in relation to storm intensity in the Atlantic basin. This is based on the hypothesis that an increase in intensity is generally associated with a greater vertical development of the cyclonic wind field associated with the vortex, which is in turn advected by an environmental flow of greater depth. Using a barotropic forecast model, the vertical extent of the environmental steering layer is varied by initializing the model with different tropospheric layer-mean wind analyses. The resultant track forecasts from 145 cases are compared to actual tracks in order to establish an optimum steering layer (a layer which best approximates verifying motion) for selected tropical cyclone intensity categories. In order to examine if the identified Atlantic relationships are universal, they are compared to relationships found in a previous study in the Australian region.

2. CASE SAMPLE

The study domain is the western North Atlantic ocean basin (roughly 10-40N, 50-100W). A total of 145 cases were examined from storms which occurred during the period 1986-1992. For a case to be included in the study sample, the following criteria had to be met: 1) 48h of subsequent storm track for verification, 2) separation of at least 24h from previous case to minimize serial correlations, 3) aircraft reconnaissance verification of storm intensity (mean sea level pressure), 4) occurring

during the months of July - October, to minimize risk of atypical storm development, structure and motion, and 5) not of subtropical or frontal development origin (atypical). The 145 cases cover a wide range of intensities from tropical depressions to severe hurricanes. Best track data supplied from the National Hurricane Center was used to verify the forecast storm tracks.

3. ANALYSIS AND FORECAST METHODOLOGY

The approach is to first create tropospheric layer-mean wind analyses from horizontal (mandatory level) wind analyses. Objective operational horizontal wind analyses were obtained from the NMC global analysis system. Selected combinations of the mandatory level wind analyses were vertically averaged by mass weighting, creating tropospheric layer-mean wind analyses (Pike 1985). The selection process was based on subjective reasoning and previous studies (e.g., Chan and Gray 1982; Dong and Neumann 1986; Velden and Leslie 1991).

Once the layer-mean analyses were completed, any apparent tropical cyclone vortex circulation was removed and replaced with the surrounding environmental flow. This methodology was chosen to focus specifically on the effects of varying the environmental flow field, and minimize the influences on the tropical cyclone motion due to vortex specifications and interactions. For a discussion of this procedure, see Velden and Leslie 1991.

The forecast module consists of two steps: 1) a nondivergent barotropic forecast of the environmental flow field, and 2) a point (storm center) trajectory forecast based on the barotropic forecast of the environmental flow. The second step is necessary because of the elimination of the vortex circulation (and associated vorticity center) as described above. The trajectory forecast begins at the specified storm center location (from best track data), and is calculated after each time step of the environmental flow forecast. This forecast procedure (see Velden and Leslie 1991 for details) is appropriate for use in our study as it provides for a track forecast based purely on the specified environmental steering current.

4. RESULTS

In each of the 145 cases, the forecast model was initialized with each of the selected layer-mean wind fields, and track forecasts were run out to 48h. The track forecast results for all of the 24h forecasts were compiled into mean forecast errors (MFE) relative to best track verification, and are shown in Table 1 (48h results were similar but not shown). The results in Table 1 are stratified into storm intensity categories in an attempt to define a relationship between the depth of the steering flow and intensity (defined as mean sea level pressure of the storm at the model initialization time). The layer-mean wind analyses in Table 1 are listed as deep tropospheric layer-means at the top, trending to low-level shallow layer-means at the bottom. Storm intensity increases by 10mb bins from left to right. Note that the number of cases in each bin generally diminishes as storm intensity increases. The lowest MFEs for each intensity bin are highlighted and indicate a definite relationship between storm intensity

Table 1. 24h mean track forecast errors (km)

Intensity Class(hPa)	1000-1010	990-999	980-989	970-979	960-969	950-959	940-949	<940
Layer Means (hPa)								
1000-100	285	240	258	258	207	368	297	327
850-200	288	233	251	256	205	366	280	311
700-200	311	292	258	272	225	351	286	<u>310</u>
850-250	276	206	248	246	194	344	<u>264</u>	332
700-250	295	256	247	248	217	345	297	323
850-300	259	194	239	253	<u>180</u>	<u>341</u>	269	340
700-300	287	230	236	244	209	359	293	324
850-400	250	168	<u>234</u>	<u>236</u>	206	367	274	339
700-400	265	201	244	252	218	372	290	337
850-500	236	<u>161</u>	242	283	210	377	273	340
700-500	250	186	247	273	228	375	284	351
850-700	<u>213</u>	178	250	294	207	378	281	364
# of Cases	(44)	(30)	(18)	(10)	(14)	(10)	(12)	(7)

and the depth of the optimum steering layer. The results show that the weaker storms are guided by a shallow, lower-tropospheric flow, while very intense hurricanes follow a deep tropospheric flow. The relationship is graphically depicted in Fig. 1. While this relationship generally follows previously determined subjective guidelines and intuitive reasoning, it is important to specifically identify the relationship in order to produce quantitative guidelines for operational use. This information can also be used to properly initialize numerical track forecast models that use tropospheric layer-mean wind analyses as input (e.g., VICBAR, BAM).

Using the guidelines in Table 1, maps or digital displays of appropriate layer-mean flow fields could be made available to operational forecasters (depending on current and forecast storm strength) as a general aid to their subjective track forecasting procedures. It should be cautioned, however, that the optimum steering layer results in Table 1 are based on an average of many cases, so that individual cases may not always follow the guidelines.

Table 2. Frequency of best 24h forecasts

Intensity Class(hPa)	1000-1010	990-999	980-989	970-979	960-969	950-959	940-949	<940
Layer-Means (hPa)								
1000-100		1		1				1
850-200	1		1				2	2
700-200							2	1
850-250	1				1	1	3	1
700-250		1	1	1	2	2	1	1
850-300	2	2	1	1	6	4	1	
700-300		1	2	1	3	1		1
850-400	1	2	5	3	1			
700-400		3	2	1				
850-500	3	11	3	1			1	
700-500	4	2	1	1		1	1	
850-700	32	7	2		1	1	1	

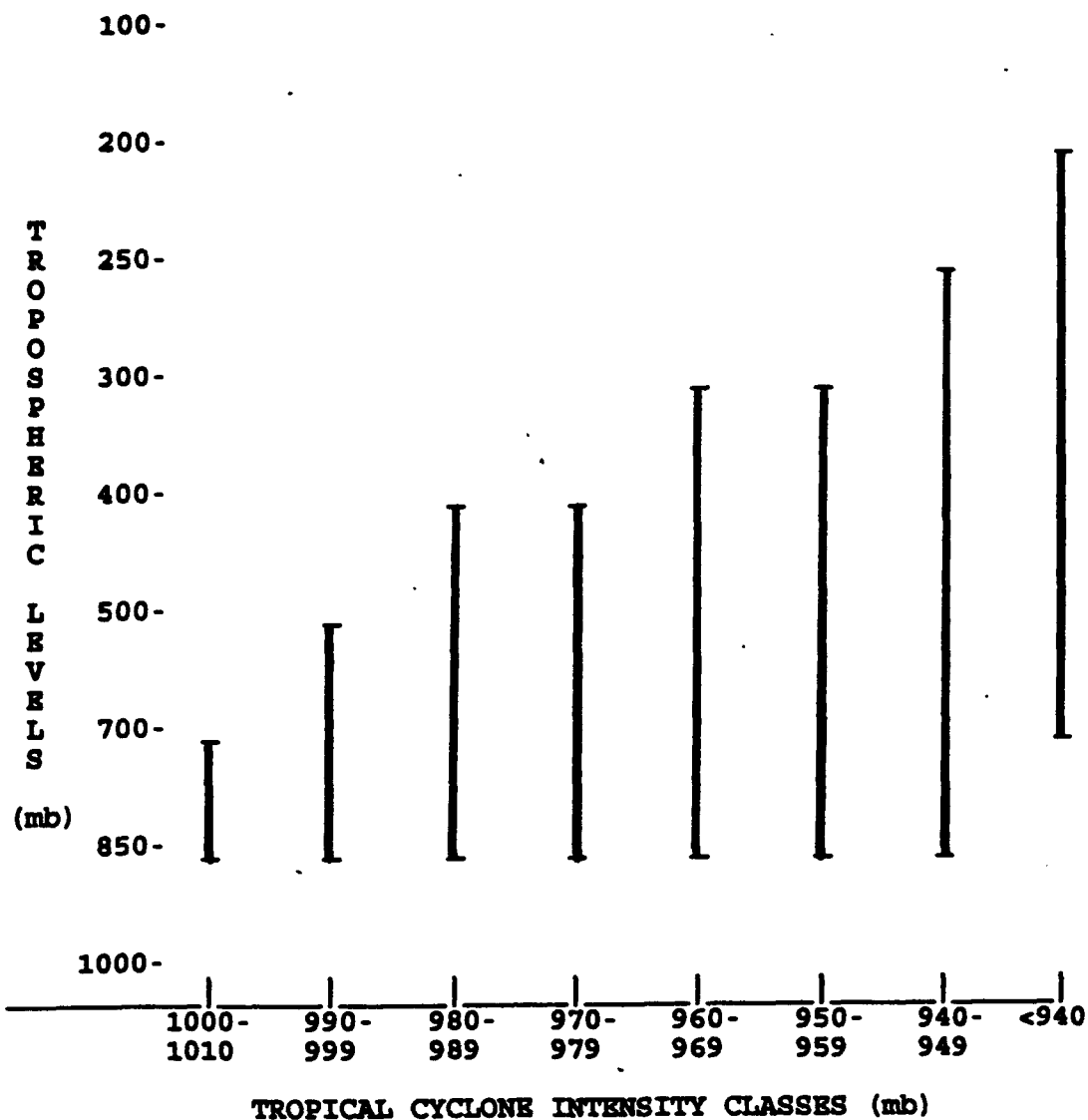


Figure 1. The relationship between tropospheric depth of the steering layer and intensity (mean sea level pressure at the center) for an Atlantic sample of tropical cyclones (based on 24h track forecast results). The black bars indicate the optimum steering layer for each intensity category.

To get an idea of the consistency of the results, Table 2 shows the frequency of optimum 24h forecasts for each layer-mean and intensity category. Although there is a spread for each intensity bin, the highest frequency of superior forecasts follows the MFE trend nicely. The few "outlier" cases (i.e. a deep layer forecast optimal for a weak storm, or a shallow layer the best forecast for an intense storm) can be attributed to; 1) cases with weak vertical and horizontal shear in the environmental flow field, 2) rapidly deepening or filling cases, or 3) model or initial analysis deficiencies. In the case of a storm imbedded in a deep laminar flow (non-sheared environment), the steering might be adequately approximated by any level or layer from 850-200mb. The relationship presented in Fig. 1 will be most useful in providing guidelines in the case of a storm in a sheared

(horizontally and/or vertically) environment.

From the relationship presented in Fig. 1, forecasters need to be aware of storms undergoing rapid intensity fluctuations. For example, a storm initially at 990mb may be following an 850-500mb flow. If the storm is forecast to rapidly deepen over the next 24h to 945mb, the 850-500 steering would no longer be appropriate 24 hrs into the track forecast (from Fig.1 and Table 1, an 850-250mb flow would, in the mean, now be optimal). A rapidly deepening system, in most cases, implies a rapid vertical spinup of the cyclonic circulation associated with the storm vortex. By our hypothesis, this deeper vortex circulation will be influenced by an environmental steering current of greater depth. The forecaster, if given adequate intensity prediction information, can take this into account in using the guidelines in Fig.1 for his/her subjective track forecast.

5. COMPARISON WITH AUSTRALIAN REGION RELATIONSHIP

The specific relationship between tropical cyclone steering layers and intensity determined in this study only applies to the Atlantic basin. It is of interest to compare the Atlantic relationship to one found in an earlier study by Velden and Leslie (1991) in the Australian region. The two findings are illustrated in Fig. 2. The black lines indicate the top (pressure) of the optimum steering layer for each intensity category (850mb is the bottom of the layer in all categories). In general terms, the relationships are similar in that the depth of the optimum steering layer increases with increasing intensity. Specifically, the Atlantic layer depth increases at a slightly faster rate with increasing intensity. It should be noted that the 850-700mb layer was not examined in the Australian study, and therefore it is possible that storms in the weakest intensity categories may have followed this layer. In addition, it was suggested in the Velden and Leslie study that Australian region cases in the severe storm category (i.e. storms with central pressures less than 925mb) followed an 850-200mb optimum steering layer. However, this was not deemed conclusive evidence based on the very limited number of cases in this intensity category.

The reasons for the subtle differences in the two relationships are beyond the scope of this paper. It is possible that structure differences between tropical cyclones in the two basins play a role. It is also possible that other basin characteristics contribute to the differences (i.e. formation and development environments, average latitude of occurrence, tropopause height, stability, etc).

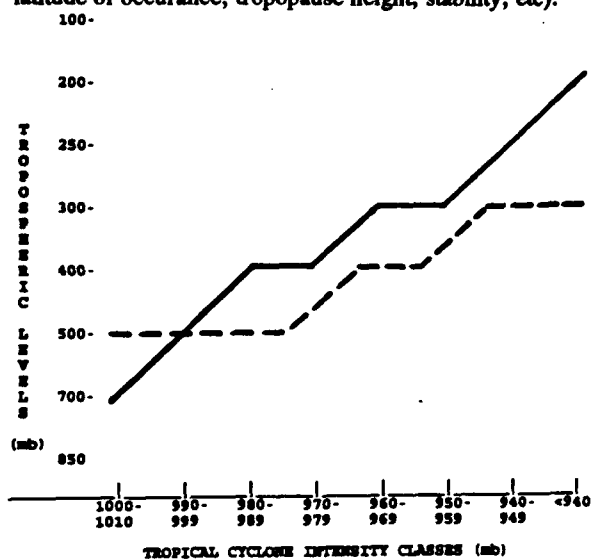


Figure 2. Comparison of tropical cyclone steering depths vs. intensity in the Atlantic and Australian basins. The lines (the Australian relationship is dashed) indicate the top of the optimum tropospheric steering layer (850mb is the bottom of the layer for all intensity categories).

6. SUMMARY

The environmental flow field around tropical cyclones accounts for a large fraction of their motion. Specifically identifying the so-called "steering current" would be very beneficial to forecasters and researchers. In this study, the tropospheric wind layer which best correlates with tropical cyclone motion in the Atlantic basin was identified for selected storm intensity categories. Supporting intuitive reasoning and subjective experience, it was found that weaker storms move with a shallow, low-level flow while the motion of intense systems is governed by deep layer-mean wind flow fields. This general relationship is explicitly established by considering 10mb storm intensity categories and using model forecast tracks to identify the optimum steering layer in each category.

The results (illustrated in Fig. 1) can be used by the operational community to provide forecasters with the necessary charts or digital-display fields, in order for them to properly assess the current and future environmental steering regimes on a case by case basis. The findings can also be used to better initialize numerical track forecast models that use layer-mean wind analyses as initial input.

It should be cautioned that the relationships found in this study are a result of approximating tropical cyclone motion with a barotropic model, on a sample of typical cases. Typical is defined here as cases where a steady environmental flow is most likely the dominating influence on storm motion. Storms undergoing other influences such as strong baroclinic interactions or land effects, or storms which develop atypically (i.e. subtropical-type storms which originate aloft and develop down to the surface), may not follow the relationships identified in this study.

Finally, the Atlantic relationship found in this study is similar to one previously found in the Australian region. In both regions, the depth of the environmental steering layer steadily increases with increasing storm intensity. The rate of increase in depth is slightly greater in the Atlantic.

7. REFERENCES

- Chan, J. and W. Gray, 1982: Tropical cyclone movement and surrounding flow relationships. *Mon. Wea. Rev.*, **110**, 1354-1374.
- Dong, K. and C.J. Neumann, 1986: The relationship between tropical cyclone motion and environmental geostrophic flows. *Mon. Wea. Rev.*, **114**, 115-122.
- Pike, A.C., 1985: Geopotential heights and thicknesses as predictors of Atlantic tropical cyclone motion and intensity. *Mon. Wea. Rev.*, **113**, 931-939.
- Velden, C.S. and L.M. Leslie, 1991: The basic relationship between tropical cyclone intensity and the depth of the environmental steering layer in the Australian region. *Wea. Forecasting*, **6**, 244-253.

Appendix 3.

Reprinted from MONTHLY WEATHER REVIEW, Vol. 119, No. 1, January 1991
American Meteorological Society

Western North Pacific Tropical Cyclone Intensity Estimation from NOAA Polar-Orbiting Satellite Microwave Data

CHRISTOPHER S. VELDEN, BRIAN M. GOODMAN AND ROBERT T. MERRILL

*Cooperative Institute for Meteorological Satellite Studies, University of Wisconsin-Madison,
Space Science and Engineering Center, Madison, Wisconsin*

(Manuscript received 15 March 1990, in final form 13 July 1990)

ABSTRACT

A method is examined for estimating the intensity of western North Pacific tropical cyclones from satellite passive microwave observations. Vertical profiles of atmospheric temperature derived from radiances remotely sensed by the Microwave Sounding Unit (MSU) onboard the current NOAA series of polar orbiting satellites are used to depict upper-tropospheric warm anomalies associated with these storms. Data from a large sample of western North Pacific tropical cyclones are used to develop a nonlinear statistical relationship between the satellite-depicted warm core anomalies and the surface intensities as measured by reconnaissance aircraft. Results based on an 82-case dependent sample indicate standard errors of 13 mb and 15 kt for estimates of the surface pressure anomalies and maximum wind speeds. These errors are reduced considerably when a bias in the sample intensity distribution is taken into account. Comparisons of results and method accuracy are made with a previous study of North Atlantic tropical cyclones.

1. Introduction

The ability of satellite-borne passive microwave radiometers to penetrate the cloudy core regions of tropical cyclones and delineate the characteristic upper-tropospheric warm anomalies has been demonstrated in numerous case studies (Rosenkranz et al. 1978; Kidder et al. 1978; Grody et al. 1979; Grody and Shen 1982). Assuming hydrostatic balance in the core region, a physical relationship should exist between the magnitude of this warm temperature anomaly and the low pressure anomaly at the surface (Kidder 1979). The technique described in this paper statistically correlates the satellite-depicted warm anomalies associated with western North Pacific tropical cyclones with surface pressure and maximum winds as measured by reconnaissance aircraft. Due to resolution limitations (110 km at nadir), the microwave observations cannot fully resolve the actual magnitude of the warm anomalies. Thus, the satellite-depicted anomalies are a volumetrically averaged representation of the true tropical cyclone anomalies. Some allowance for undetected warming due to the coarse data resolution is implicit in the statistics.

A similar method for estimating tropical cyclone intensity in the Atlantic was developed by Velden (1989). This study presented a detailed qualitative description of MSU applications on a large sample of North At-

lantic cases and expands upon previous work (Kidder et al. 1978; Velden and Smith 1983) in developing quantitative relationships between the satellite-observed upper-tropospheric thermal anomaly and reconnaissance-measured surface intensity. Correlations were found to be good with standard errors of 8 mb and 13 kt for estimates of surface pressure and maximum wind speeds.

With the discontinuance of aircraft reconnaissance missions into western North Pacific tropical cyclones, alternate techniques to monitor storm intensity over this region are needed. The Dvorak technique (Dvorak 1975, 1984), which is a pattern recognition scheme that uses visible and infrared satellite imagery, is employed operationally worldwide. While this scheme works well in most cases, it has limitations (Kidder 1979) and is not purely objective. Most notably, tropical cyclones undergoing rapid intensity changes are underestimated (Martin 1988). The standard errors of estimate for the microwave technique developed in the Atlantic by Velden (1989) are comparable to the Dvorak method, and has the additional quality of being fully objective. It is desirable for operational centers to have independent objective guidance available in questionable situations.

The emphasis of this paper is on the ability of the NOAA satellite MSU data (Smith et al. 1979) to provide estimates of western North Pacific tropical cyclone intensity. MSU satellite observations were obtained during 82 cases of western North Pacific tropical cyclones in 1980, 1983, and 1984. As in Velden (1989), quantitative relationships are statistically derived and

Corresponding author address: Mr. Christopher S. Velden, CIMSS, University of Wisconsin—Madison, 1225 W. Dayton Street, Madison, WI 53706.

evaluated for their potential as operational schemes. The models developed on Pacific cases in this study are then compared with those previously developed on Atlantic cases.

2. Data sample

The datasets utilized in this study consist of Microwave Sounding Unit observations from the NOAA series polar-orbiting satellites, and ground truth provided by western North Pacific aircraft reconnaissance, post-analysis "best-track" maximum wind estimates, and operational surface pressure analyses.

The NOAA polar orbiter satellites in operation during this period were TIROS-N, NOAA-6, NOAA-7 and NOAA-8. Satellite overpasses of western North Pacific tropical cyclones from 1980 through 1984 were requested from the NOAA Satellite Data Services Division (SDSD) that fit the following criteria: 1) a reconnaissance observation was available near the time of the satellite overpass of the tropical cyclone; and 2) the tropical cyclone was well centered in the satellite overpass (not more than $\sim 6^\circ$ longitude from the satellite subpoint, corresponding to a $\sim 28^\circ$ satellite zenith angle). The second criterion was also applied by Kidder (1979) and Velden (1989), because of the degradation of resolution, calculated transmittance functions, and resulting sounding information toward the limbs of the overpass. Unfortunately, NOAA polar orbiting data from 1981 and 1982 were not available from SDSD. Overpasses for 82 cases that satisfied the above criteria from 1980, 1983, and 1984 constitute the data sample.

Air Force reconnaissance center fixes of western North Pacific tropical cyclones for the period 1980 through 1984 were compiled at Colorado State University. Each fix provides location and minimum sea level pressure. Surface pressure anomalies are derived by subtracting the reconnaissance measured central pressure from the environmental surface pressure surrounding the storm, which is determined from operational western Pacific surface analyses on archive at the University of Wisconsin. This surface pressure anomaly (ΔP_{sfc}) is one of the regressands in the statistical relationships developed in section 4. Another regressand, the maximum wind (V_{max}), is determined from postanalyzed storm "best tracks," which were obtained from the Naval Environmental Prediction Research Facility (direct observations of maximum wind by reconnaissance aircraft are not used due to measurement variability associated with asymmetries in the wind field).

3. Method

Two options are available for representing the tropical cyclone warm core anomaly with NOAA satellite microwave measurements: 1) the 54.96-GHz (MSU channel 3) radiance anomaly (ΔR_3 , core value minus an average environmental value) and 2) the retrieved

temperature anomaly (core minus environment) at the 250-mb level (ΔT_{250}) as determined from processed microwave soundings. The 54.96-GHz channel senses peak radiances emitted near the level of maximum warming in the core of western North Pacific tropical cyclones (Nunez and Gray 1977). Some examples of this product in smoothed imagery format are presented in Fig. 1. The retrieved temperature anomaly at 250 mb (the closest mandatory level to the climatological level of maximum warming) is a result of vertical soundings produced from the physical iterative solution of Smith (1970), which takes advantage of all four microwave channels (no infrared channels are utilized in this application), and includes precipitation attenuation checks. Anomalies are determined interactively on the Man computer Interactive Data Access System (Suomi et al. 1983) by taking the value (either R_3 or T_{250}) at the location of the tropical cyclone center and at ten locations surrounding the tropical cyclone cloud system (typically at a 600–1000 km radius). The ten environmental values are averaged, and then subtracted from the center value to derive the respective ΔR_3 or ΔT_{250} quantities. A detailed description may be found in Velden and Smith (1983).

To determine which of the two satellite parameters best correlates with surface intensity, a linear regression analysis is applied to the 82 cases, and ΔP_{sfc} is related to each parameter. It is found that ΔT_{250} explains about 73% of the observed variance, while ΔR_3 explains 68%. For V_{max} , ΔT_{250} explains 65% of the observed variance, while ΔR_3 explains 58%. Based on these results, the remainder of the study will focus on the ΔT_{250} parameter.

An additional experiment is performed to test for the impact of precipitation attenuation on the microwave retrievals. The 54.96-GHz channel radiances (maximum sensitivity near 250 mb) are not severely affected by precipitation attenuation because hydrometeors in convection at these heights are usually in the form of ice, which is mostly transparent to this wavelength. Because MSU channels 1 and 2 (50.3 and 53.7 GHz, respectively) are affected by heavy rain, and since these channels are used in the physical retrieval algorithm (and might affect the core ΔT_{250} value), a correction for this attenuation must be applied. Two correction methods are examined. The first involves manually editing suspect radiances from the field, and replacing them with interpolated values from surrounding radiances unaffected by precipitation. This is a rather cumbersome task and involves some subjectivity. The second method simply relies on the internal checks in the retrieval scheme (Smith 1970) to objectively correct for any precipitation attenuation. A fortunate result from an operational standpoint (ease of application) is that the ΔT_{250} core values from the second method yield slightly superior results when correlated with ΔP_{sfc} . These values are used in the relationships developed below.

4. Results

Several classes of statistical models relating the observed surface intensity and the satellite-depicted warm anomaly are derived. The basic model involves a simple linear relationship between surface intensity and the satellite-derived ΔT_{250} . A modification of this basic model is examined next, which includes the addition of nonlinear and latitude terms. It is found that our 82 case sample contains a high intensity bias relative to western North Pacific climatology, most likely due to our constraint that reconnaissance be available. Since this intensity estimation technique has potential operational applications, an estimate of this method's performance on a population adjusted to more appropriately represent climatology is given.

First consider the simplest regression models developed on the 82 case sample. The details of the model coefficients are given in Tables 1 and 2. For estimating ΔP_{sfc} , the simple linear model (sequence 1 in Table 1) yields a standard error of just over 14 mb. For ΔT_{250} values greater than about 5°C, the relationship appears to acquire a nonlinear component (Fig. 2). To allow for this nonlinearity, a stepwise multiple regression is used to select coefficients of a low-order polynomial that are significant above the 95% confidence limit. For both ΔP_{sfc} and V_{max} , a quadratic function of ΔT_{250} was found to yield the "best" fit (sequence 2). The additional term $(\Delta T_{250})^2$ provides a scalable curvature adjustment that has a minimal impact on low values of ΔT_{250} , and reduces the intensity estimates for large values of ΔT_{250} .

A second nonlinear term ($\Delta T_{250} \times \text{LAT}$), which accounts for the variance in ΔT_{250} with latitude (discussed in Velden 1989), is also found to provide statistically significant information to the model. The overall error is reduced by nearly 1/2 mb when latitude information is incorporated into the model (sequence 3 in Table 1). The final model, which includes all linear and nonlinear terms (sequence 4 in Table 1), results in a reduction of the standard error to 13.2 mb.

The regression models for estimating V_{max} follow a similar development to ΔP_{sfc} and are shown in Table 2. The linear model yields a standard error of 17.3 kt, which is reduced to 15.4 kt when the nonlinear terms are incorporated into the model. The correlations for the ΔT_{250} versus V_{max} relationships are slightly below that of ΔT_{250} versus ΔP_{sfc} . This is likely a result of the fact that temperature anomalies and ΔP_{sfc} are directly related through hydrostatic balance, while V_{max} is related to the local gradient of surface pressure, and less directly to ΔP_{sfc} .

It was mentioned earlier that our data sample is biased towards stronger storms. An evaluation of the accuracy (and operational potential) of this technique is dependent upon the distribution of storm intensities within the data sample (higher intensities will lead to inherently higher variability). Since this method has

potential operational applications, it is of interest to examine our 82 case sample relative to a more representative intensity distribution. Fourteen years of western North Pacific best-track wind speed data (1973–86) were available to estimate a more representative climatology of typhoon intensity. Best-track information from the three years of our 82 case sample (1980, 1983, 1984) is specifically used to estimate any linear biases in our 82 case storm intensity distribution. Frequency distributions (Fig. 3) of western North Pacific tropical cyclone intensity (defined as best-track wind speed estimates) indicate that the 82 case sample is biased towards higher wind speed cases. The average wind speed for the 82 case sample is 73 kt, compared to 52 kt for the 3-yr sample and 50 kt for the 14-yr sample. This strong bias is most likely the result of our cases being constrained to those having coincident reconnaissance reports. Climatological samples will contain a plethora of weak or developing cases not investigated by aircraft, which lowers the average wind speeds of these samples relative to our sample. This bias affects the nature of the error characteristics of the intensity estimation technique presented in this study. Since the model shows less variance in the weaker storm cases (Fig. 2), an adjustment to a climatologically representative sample should result in a lower overall model standard error of estimate relative to sequence 4 of Tables 1 and 2.

The model coefficients are rederived to reflect an adjustment of the sample intensity distribution to be more in line with a climatological distribution from the years in which our cases were sampled (1980, 1983, and 1984). The regression model coefficients and error statistics corresponding to the climatological intensity distribution are derived from the original regression coefficients and error statistics using the mean and standard deviation of the original regression residuals, and the relative percentages of the original and climatological distributions (Steel and Torrie 1960). The resulting models for ΔP_{sfc} and V_{max} are given in sequence 5 of Tables 1 and 2, respectively. It is notable that the equations change very little. However, the standard errors are 1.8 mb and 2 kt lower than the comparable errors on our original 82 case sample (sequence 4 in Tables 1 and 2). This reflects the effect of including a larger percentage of weaker storms, which have inherently less variability in the development of the model relationships, and provides a more representative evaluation of the expected model accuracy in an operational mode.

As was noted in Velden (1989), the slopes of the ΔT_{250} versus ΔP_{sfc} relationships are dependent upon how fully the warm anomaly is resolved by the satellite. The broader the horizontal extent of a warm core with a large component above the melting level, the more fully resolved it will be in the MSU observations. Therefore, the ΔT_{250} for a large/filling typhoon having a given observed ΔP_{sfc} will be greater than that observed

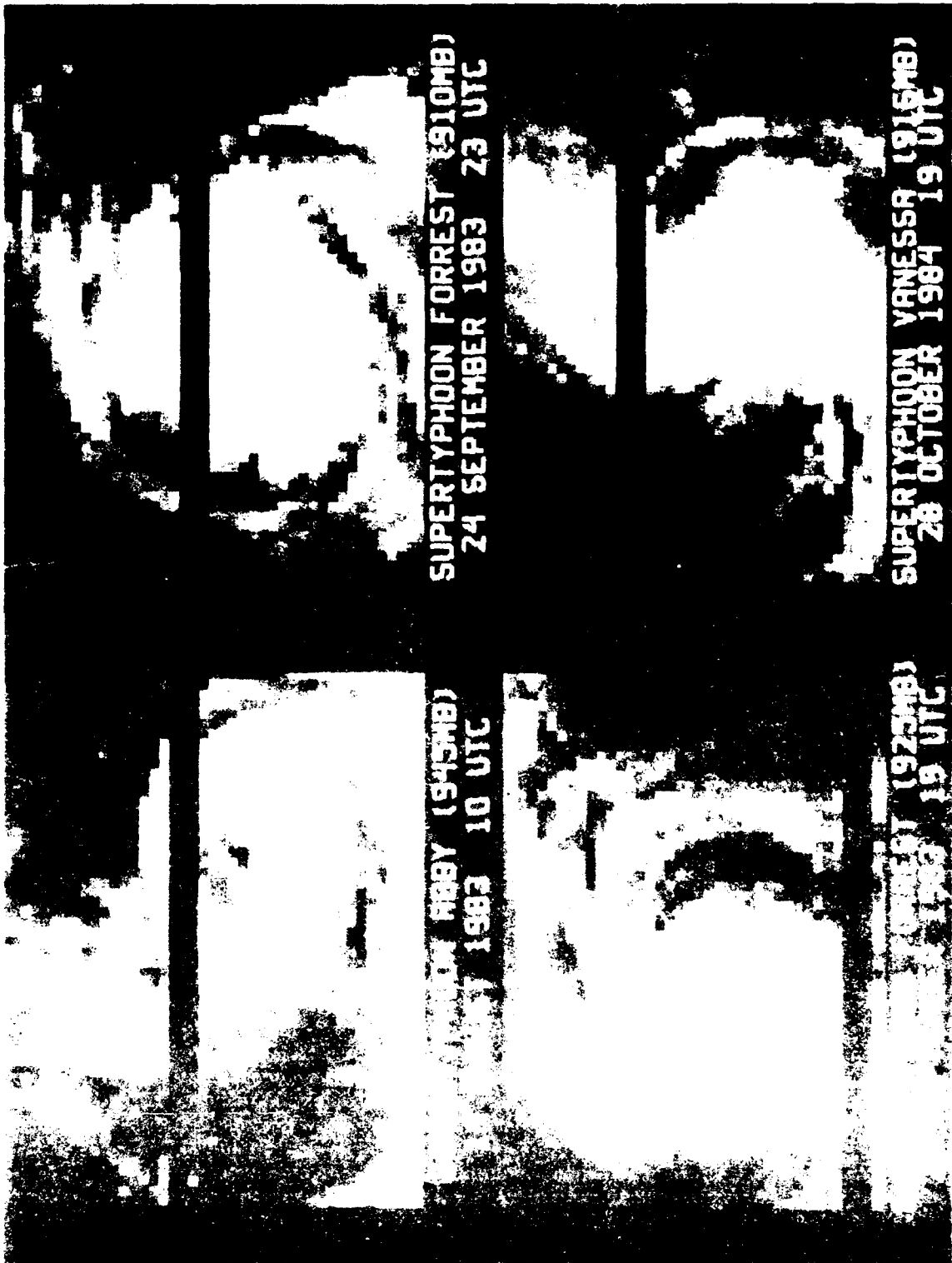


FIG. 1. (a) Tropical storm Abby (1945 mb) on 23 September 1983, 10 UTC. (b) Super typhoon Forrest (910 mb) on 24 September 1983, 23 UTC. (c) Super typhoon Vanessa (915 mb) on 28 October 1984, 19 UTC. (d) Tropical storm Forrest (925 mb) on 28 October 1984, 19 UTC. The images were obtained from the Advanced Very High Resolution Radiometer (AVHRR) on the Tropical Rainfall Measuring Mission (TRMM) satellite. The images were processed using the TRMM software package.

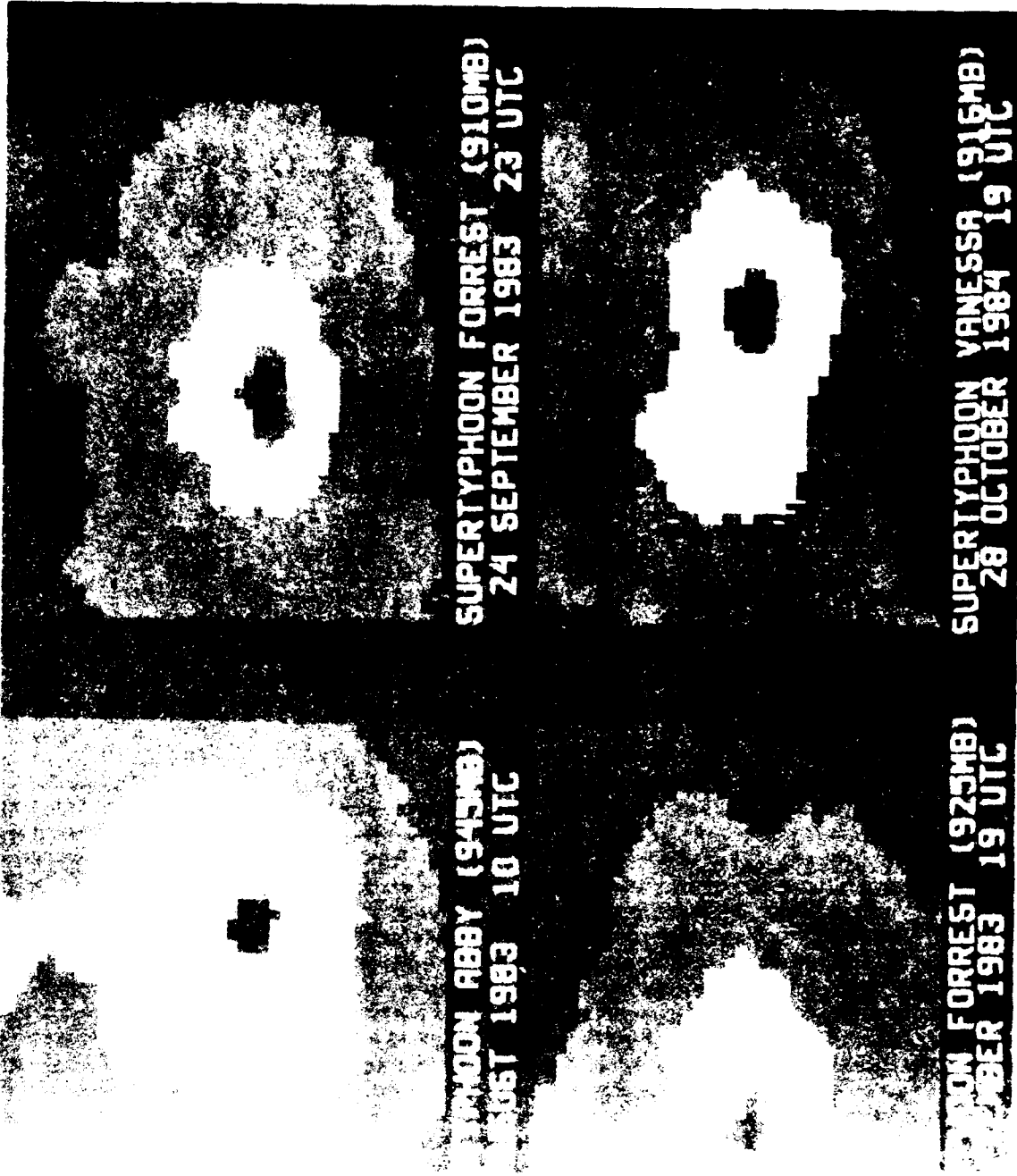


TABLE 1. Coefficients and error characteristics for the relationship between ΔT_{250} and ΔP_{sfc} on the full 82 case sample. R^2 is the fraction of explained variance and SE is the standard error of estimate (mb). The sample average and standard deviation for ΔP_{sfc} are 41 and 27 mb, respectively. The final relationship (sequence 5) is rederived from an adjusted sample based on a climatological intensity distribution.

Sequence	Variable	Coefficient	R^2	SE
1	Constant	8.26	0.73	14.1
	ΔT_{250}	9.18		
2	Constant	1.79	0.75	13.7
	ΔT_{250}	13.28		
	$(\Delta T_{250})^2$	-0.42		
3	Constant	6.31	0.76	13.5
	ΔT_{250}	13.28		
	$\Delta T_{250} \times \text{LAT}$	-0.16		
4	Constant	.16	0.76	13.2
	ΔT_{250}	17.09		
	$(\Delta T_{250})^2$	-0.41		
	$\Delta T_{250} \times \text{LAT}$	-0.16		
5	Constant	-0.51	0.81	11.4
	ΔT_{250}	17.21		
	$(\Delta T_{250})^2$	-0.42		
	$\Delta T_{250} \times \text{LAT}$	-0.15		

in a small, deepening system of equal intensity. This is apparently the cause of the nonlinearity at ΔT_{250} values greater than about 5°C . Most of these cases have been identified as "filling" storms (Fig. 2), which typically exhibit broader warm core structures (Miller 1964; Sheets 1968; Shea 1972; Hawkins and Imbembo 1976), and a smaller percentage of warming in the eye below the melting level (Jordan 1961). They are therefore more able to be consistently resolved by the relatively coarse satellite observations. Thus, the sensitivity of our sample to storm stage could account for the seemingly different relationship with $\Delta T_{250} > 5^\circ\text{C}$.

To summarize, the dominant underlying relationship involves a linear increase in surface intensity with ΔT_{250} . The addition of the supplementary nonlinear predictors [$(\Delta T_{250})^2$ and $\Delta T_{250} \times \text{LAT}$] reduces the standard errors for both ΔP_{sfc} and V_{\max} model estimates. The improvements due to each additional term are statistically significant above the 95% level. The additional nonlinear terms provide a source of curvature to the model which have the effect of moderating the surface intensity estimates for large ΔT_{250} values and increasing latitudes, while having a minimal impact on intensity estimates for small ΔT_{250} values. The effects of these terms also contribute some physical insight, since the statistical relationships implicitly include the effects of the coarse MSU horizontal resolution. For example, larger central warm cores will be better resolved in the MSU signal. By including these nonlinear terms into the regression models, some of the variance in the basic upper-level warm core versus surface intensity relationship is explained.

5. Comparison of Pacific versus Atlantic results

It is interesting to compare the results of the method on western North Pacific cases presented in this study with the results on Atlantic cases found in Velden (1989). The range of the satellite-derived ΔT_{250} values in the Pacific sample is nearly twice that of the Atlantic sample (0° – 11°C versus 0° – 5°C), even though the relative difference in range of ΔP_{sfc} is much less (0–105 mb versus 0–80 mb). This finding is most likely a result of the fact that the mean typhoon is twice as large in area as the mean hurricane (Merrill 1984), allowing typhoon warm anomalies (which are typically 1.5 times stronger than hurricane anomalies, Nunez and Gray 1977) to be more fully resolved by the MSU observations.

a. Basic relationships

Only the linear model from this study may be compared since only linear models were evaluated in the Atlantic study. In addition, only the cases with $\Delta T_{250} \leq 5^\circ\text{C}$ are used (66 cases), since beyond this range the relationship becomes nonlinear, and also comparable Atlantic cases did not exist in the Velden (1989) study.

The basic linear relationships for 103 Atlantic cases found in Velden (1989) are

$$\Delta P_{sfc} = 17.5\Delta T_{250} - 2 \quad (\text{mb})$$

$$V_{\max} = 28.0\Delta T_{250} + 18 \quad (\text{kt}).$$

The basic linear relationships for the 66 western North Pacific cases are

$$\Delta P_{sfc} = 11.8\Delta T_{250} + 2 \quad (\text{mb})$$

$$V_{\max} = 13.0\Delta T_{250} + 32 \quad (\text{kt}).$$

TABLE 2. Coefficients and error characteristics for the relationship between ΔT_{250} and V_{\max} on the full 82 case sample. R^2 is the fraction of explained variance and SE is the standard error of estimate (kt). The sample average and standard deviation for V_{\max} are 73 and 29 kt, respectively. The final relationship (sequence 5) is derived from an adjusted sample based on a climatological intensity distribution.

Sequence	Variable	Coefficient	R^2	SE
1	Constant	40.35	0.65	17.3
	ΔT_{250}	9.23		
2	Constant	30.72	0.67	16.7
	ΔT_{250}	15.32		
	$(\Delta T_{250})^2$	-0.63		
3	Constant	37.65	0.68	16.5
	ΔT_{250}	14.92		
	$\Delta T_{250} \times \text{LAT}$.23		
4	Constant	28.46	0.70	15.4
	ΔT_{250}	20.61		
	$(\Delta T_{250})^2$	-0.60		
	$\Delta T_{250} \times \text{LAT}$	-0.22		
5	Constant	24.63	0.79	13.4
	ΔT_{250}	21.30		
	$(\Delta T_{250})^2$	-0.61		
	$\Delta T_{250} \times \text{LAT}$	-0.21		

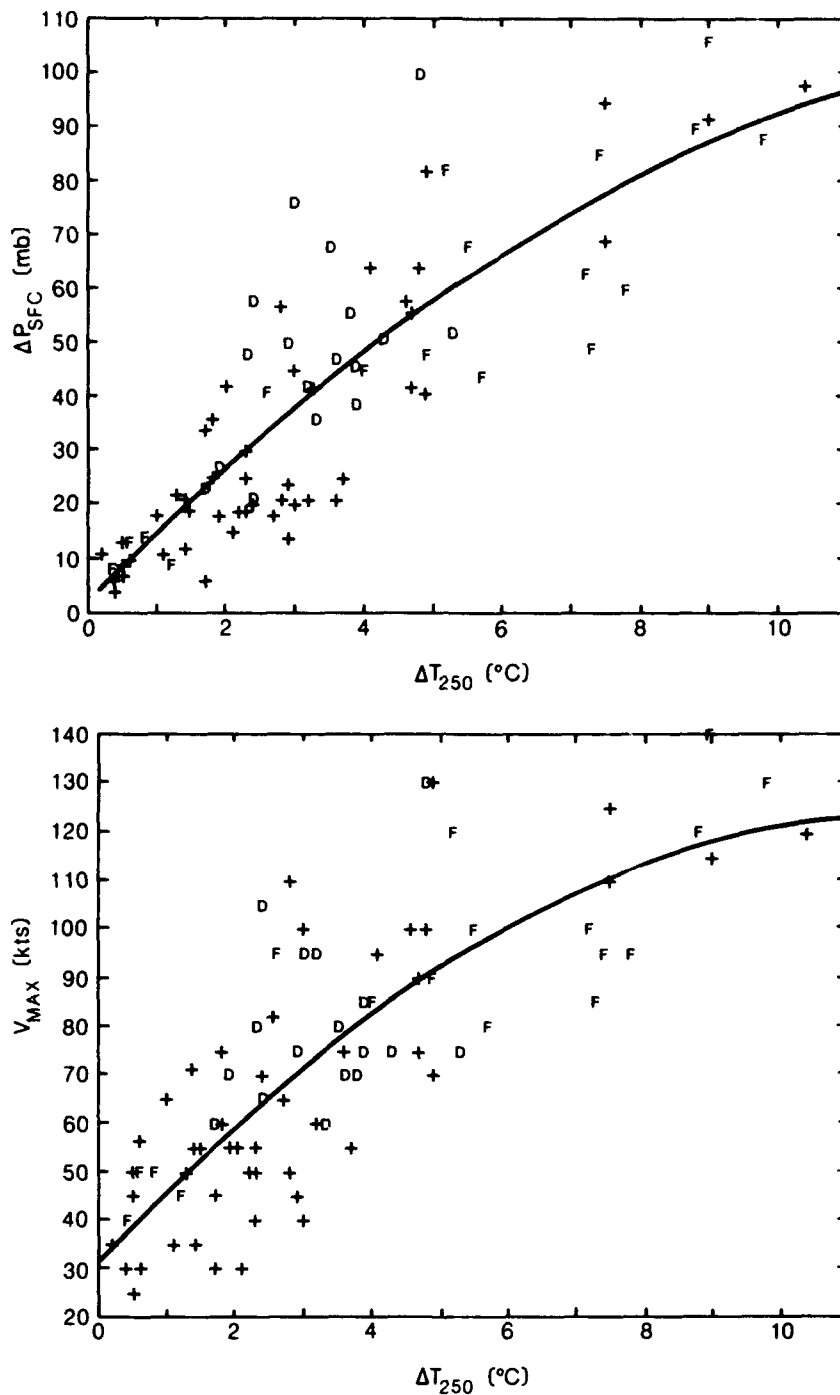


FIG. 2. (a) Scatter plot of the 250-mb satellite-derived temperature anomaly (ΔT_{250}) and the surface pressure anomaly (ΔP_{SFC}) in western North Pacific tropical cyclones. (b) As in (a), except for (ΔT_{250}) versus V_{MAX} , where V_{MAX} is the maximum sustained surface winds from best-track data. D represents steady deepener and F represent steady filler.

The marked differences in the two relationships (Fig. 4) confirm the assertion in Velden (1989) that the relationships developed in the Atlantic may not hold in

other tropical cyclone basins. For example, a ΔT_{250} value of 5°C yields 85 mb/158 kt in the Atlantic, and 61 mb/97 kt in the Pacific for ΔP_{SFC} and V_{MAX} , respec-

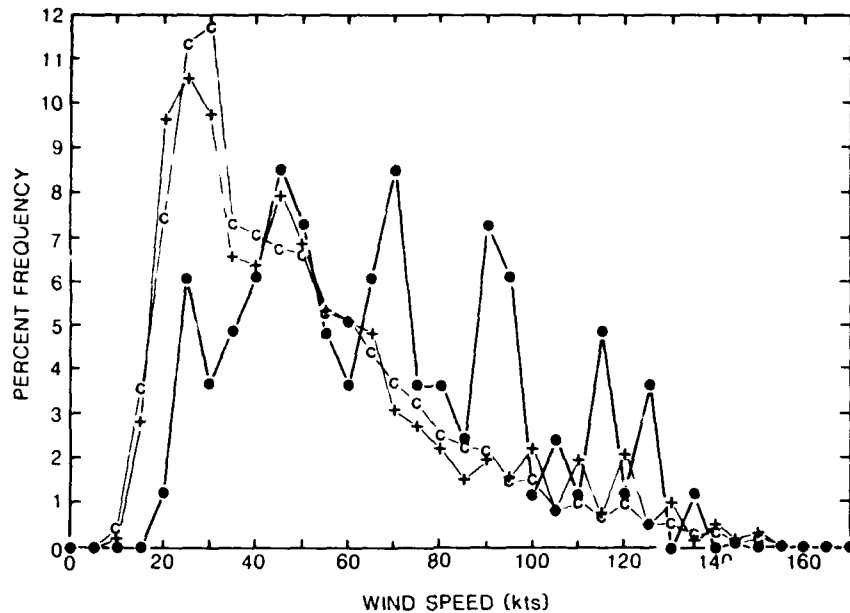


FIG. 3. Distribution of western North Pacific tropical cyclone intensities (best-track wind speeds) as a function of percent frequency for the period 1973-86 (C), the years 1980, 1983, and 1984 (+), and for our 82 case sample (●).

tively. This implies basic structural differences in the thermal anomalies and environments between Atlantic hurricanes and western North Pacific typhoons.

b. Error characteristics

For the 103 Atlantic cases in Velden (1989), the standard error and explained variance for the estimate of ΔP_{stc} are 8 mb and 0.83. For the estimate of V_{max} , the respective values are 13 kt and 0.79. The Pacific error values (66 case sample) are 13 mb and 0.59 for the ΔP_{stc} standard error and fraction of explained variance, and 17 kt and 0.52 for the respective V_{max} estimates. The technique seems to do better in the Atlantic. This may, in part, be due to the sample intensity distributions. The Pacific sample contains a greater proportion of stronger intensity cases, which would inherently lead to higher standard errors. The average ΔP_{stc} in the Atlantic sample is 28 mb, while in the Pacific sample it is 41 mb. In addition, the Pacific sample contains more cases of rapid intensity change events, which results in more inconsistent measurements of the warm core (ΔT_{250}) by the satellite and consequently larger standard errors.

6. Discussion

A method is presented to estimate western North Pacific tropical cyclone intensity using microwave observations from NOAA polar-orbiter satellites. The de-

rived statistical relationships on a 82-case sample yield standard errors of around 13 mb and 15 kt for estimates of the surface pressure anomaly and maximum wind speeds. These errors are estimated to be approximately 11 mb and 13 kt given a more representative western North Pacific tropical cyclone intensity distribution.

Further examination of the individual cases reveals that storm structure and stage is an important factor in the ability of the MSU to consistently resolve the upper-level warm anomaly. The method appears to be most reliable when applied to storms characterized by large eyes and/or rising pressure tendencies. In deepening systems (especially rapidly deepening systems), the characteristic concentrated warm core is inconsistently resolved by the MSU observations, resulting in higher standard errors. This is an unfortunate result given the particular need for a technique that works well in rapidly deepening situations.

An inherent weakness of the technique is the use of a single temperature level (250 mb) to infer the magnitude of the warm anomaly. It is likely that the level (and integrated depth) of maximum warming will vary in individual cases depending on intensity, latitude, environmental conditions, etc. Since the vertical resolution of the MSU data is quite coarse, it is difficult to determine the actual level of peak warming in each case. For this reason, a fixed level (250 mb) based on composite analyses (Nunez and Gray 1977) was utilized in this study, and certainly introduces variance into the model.

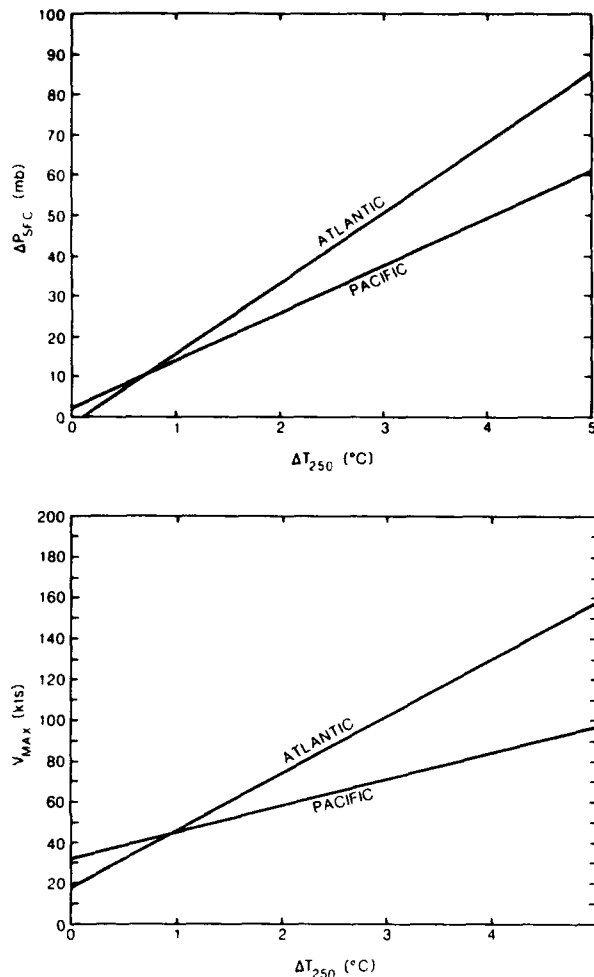


FIG. 4. Linear models derived from Atlantic and western North Pacific tropical cyclone data sets for a) ΔT_{250} versus ΔP_{SFC} , and b) ΔT_{250} versus V_{MAX} .

Despite the limitations, the accuracy of the intensity estimates using this technique suggests that it could be used operationally to supplement the Dvorak scheme. The 11-mb standard error (adjusted sample) for surface intensity estimates is comparable to the 9-mb standard error of the Dvorak scheme in western North Pacific typhoons (Martin 1988). Martin notes that this 9-mb figure may be conservative because the Dvorak satellite classifications are frequently known not to be independent of available aircraft intensity measurements. Unlike the Dvorak scheme, the proposed microwave technique is purely objective and is not influenced by previous estimates. Intensity estimates could be obtained as often as four times per day with a two-satellite configuration. However, the need to have the storm relatively well centered in the overpass will somewhat limit this availability. An adequate interactive satellite data processing system will be necessary to ingest the

data and derive microwave soundings in a timely fashion.

7. Future work

It is important that the abilities and limitations of the current observing systems in specific applications be well documented to address the needs and designs of future instruments (Shenk et al. 1987). The standard errors of the statistical models in this study could be reduced using higher resolution microwave data such as will be provided by the Advanced Microwave Sounding Unit (AMSU), which is to be deployed in 1992. Unfortunately, a statistical study using AMSU data on western North Pacific storms will not be possible since reconnaissance "ground truth" data will not be available. However, a physical intensity retrieval model is currently being developed that will be tested on our MSU sample. This method analytically models the horizontal thermal structure of the typhoon's upper-troposphere and retrieves the structural parameters of the model (i.e., ΔT_{250}) from nearby microwave measurements by inversion of the radiative transfer equation. In this scheme, the coarse horizontal resolution of the radiometer is explicitly taken into account. We hope this model will be the prototype for future typhoon intensity estimation schemes using more advanced microwave radiometers.

Acknowledgments. The authors wish to thank Drs Robert Abbey, Ken Hardy, and Mort Glass for providing financial support of this project under ONR Contract N00014-88-K-0711. Appreciation is extended to Dr. Bill Gray for providing reconnaissance data, Dr. Ted Tsui for providing best-track information, Russ Elsberry and an anonymous reviewer for providing helpful suggestions, and Laura Beckett for preparing the manuscript.

REFERENCES

- Dvorak, V. F., 1975: Tropical cyclone intensity analysis and forecasting from satellite imagery. *Mon. Wea. Rev.*, **103**, 420-430.
- , 1984: Tropical cyclone intensity analysis using satellite data. NOAA Tech. Rep. NESDIS 11, National Environmental Satellite Data Information Service, Washington, DC, 47 pp.
- Grody, N., and W. C. Shen, 1982: Observations of Hurricane David (1979) using the microwave sounding unit. NOAA Tech. Rep. NESD 88, NESDIS, Washington, DC, 52 pp.
- , C. M. Hayden, W. C. Shen, P. W. Rosenkranz and D. G. Staelin, 1979: Typhoon June winds estimate from scanning microwave spectrometer measurements at 55.45 GHz. *J. Geophys. Res.*, **84**, 3689-3695.
- Hawkins, H. F., and S. M. Imbembo, 1976: The structure of a small intense hurricane—Inez 1966. *Mon. Wea. Rev.*, **104**, 418-442.
- Jordan, C. L., 1961: Marked changes in the characteristics of the eye of intense typhoons between the deepening and filling stages. *J. Appl. Meteor.*, **18**, 779-789.
- Kidder, S. Q., 1979: Determination of tropical cyclone pressure and

- winds from satellite microwave data. Atmos. Sci. Paper No. 317, Colorado State University, Fort Collins, CO, 87 pp.
- , W. M. Gray and T. H. Vonder Haar, 1978: Estimating tropical cyclone central pressure and outer winds from satellite microwave data. *Mon. Wea. Rev.*, **106**, 1458–1464.
- Martin, J., 1988: Tropical cyclone observation and forecasting with and without aircraft reconnaissance. Atmos. Sci. Paper No. 428, Colorado State University, Fort Collins, CO, 114 pp.
- Merrill, R. T., 1984: A comparison of large and small tropical cyclones. *Mon. Wea. Rev.*, **112**, 1408–1418.
- Miller, B. I., 1964: A study of the filling of Hurricane Donna (1960) over land. *Mon. Wea. Rev.*, **92**, 389–406.
- Nunez, E., and W. M. Gray, 1977: A comparison between West Indies hurricanes and Pacific typhoons. *Proc. 11th Tech. Conf. on Hurricane and Tropical Meteorology*, Miami, Amer. Meteor. Soc., 528–534.
- Rosenkranz, P. W., D. H. Staelin and N. C. Grody, 1978: Typhoon June (1975) viewed by a scanning microwave spectrometer. *J. Geophys. Res.*, **83**, 1857–1868.
- Shea, D. J., 1972: The structure and dynamics of the hurricane's inner core region. Atmos. Sci. Paper No. 182, Colorado State University, Fort Collins, CO, 134 pp.
- Sheets, R. C., 1968: The structure of Hurricane Donna (1964). ESSA Tech. Memo. ERL TM-NHRL 83, AOML-HRD, Miami, 64 pp.
- Shenk, W. E., T. H. Vonder Haar and W. L. Smith, 1987: An evaluation of observations from satellites for the study and prediction of mesoscale events and cyclone events. *Bull. Amer. Meteor. Soc.*, **68**, 21–35.
- Smith, W. L., 1970: Iterative solution of the radiative transfer equation for temperature and absorbing gas profiles of an atmosphere. *Appl. Optics*, **9**, 1993–1999.
- , H. M. Woolf, C. M. Hayden, D. Q. Wark and L. M. McMillin, 1979: The TIROS-N operational vertical sounder. *Bull. Amer. Meteor. Soc.*, **60**, 1177–1187.
- Steel, R. G. D., and J. H. Torrie, 1960: *Principles and Procedures of Statistics*. McGraw-Hill, 481 pp.
- Suomi, V. E., R. Fox, S. S. Limaye and W. L. Smith, 1983: McIDAS III: A modern interactive data access and analysis system. *J. Climate Appl. Meteor.*, **22**, 765–778.
- Velden, C. S., 1989: Observational analyses of North Atlantic tropical cyclones from NOAA polar-orbiting satellite microwave data. *J. Appl. Meteor.*, **28**, 59–70.
- , and W. L. Smith, 1983: Monitoring tropical cyclone evolution with NOAA satellite microwave observations. *J. Climate Appl. Meteor.*, **22**, 714–724.

Appendix 4.

Reprinted from WEATHER AND FORECASTING, Vol. 6, No. 2, June 1991
American Meteorological Society

**The Basic Relationship between Tropical Cyclone Intensity and the Depth
of the Environmental Steering Layer in the Australian Region**

CHRISTOPHER S. VELDEN

LANCE M. LESLIE

The Basic Relationship between Tropical Cyclone Intensity and the Depth of the Environmental Steering Layer in the Australian Region

CHRISTOPHER S. VELDEN

Cooperative Institute for Meteorological Satellite Studies, University of Wisconsin-Madison, Madison, Wisconsin

LANCE M. LESLIE

Australian Bureau of Meteorology Research Centre, Melbourne, Victoria, Australia

(Manuscript received 16 October 1990, in final form 30 January 1991)

ABSTRACT

A simple barotropic model is employed to investigate relative impacts on tropical cyclone motion forecasts in the Australian region when wind analyses from different tropospheric levels or layers are used as the input to the model. The model is initialized with selected horizontal wind analyses from individual pressure levels, and vertical averages of several pressure levels (layer-means).

The 48-h mean forecast errors (MFE) from this model are analyzed for 300 tropical cyclone cases that cover a wide range of intensities. A significant reduction in the track forecast errors results when the depth of the vertically-averaged initial wind analysis depends upon the initial storm intensity. Mean forecast errors show that the traditionally-utilized 1000–100-hPa deep layer-mean (DLM) analysis is a good approximation of future motion only in cases of very intense tropical cyclones. Shallower, lower-tropospheric layer-means consistently outperform single-level analyses, and are best correlated with future motion in weak and moderate intensity cases.

These results suggest that barotropic track forecasting in the Australian region can be significantly improved if the depth of the vertically-averaged initial wind analysis is based upon the tropical cyclone intensity.

1. Introduction

There is little question that the environmental flow accounts for a large fraction of tropical cyclone motion (Elsberry et al. 1987). Previous studies of the steering concept concluded that tropical cyclone motion could best be approximated by either a mid-tropospheric level (500 or 700 hPa), or a mass-weighted deep layer-mean (DLM) flow field such as the vertically-averaged wind over the 1000–100-hPa layer. However, operational hurricane forecasters know from experience that, in general, weaker tropical cyclones move with a shallow lower-tropospheric flow while the more well-developed systems move with a deep-layer flow (Simpson 1971). The background on the development of environmental steering concepts is summarized in Elsberry et al. (1987).

The question pertaining to the optimum level, or layer, which best approximates tropical cyclone motion was quantitatively addressed by Dong and Neumann (1986). They found that the optimum depth of the deep layer for steering Atlantic hurricanes is greater

than that for weaker tropical storms, and that deep-layer steering is generally better than single-level steering (in agreement with Pike 1987). Chan and Gray (1982) examined cases from three tropical cyclone basins including the Australian region, in which they documented the deviations of storm motion from selected levels/layers of environmental steering. Deep-layer steering was found to be a good descriptor of cyclone movement. These studies suffered somewhat from generality in that only broad intensity classes (tropical storm and hurricane) were considered.

In this paper we expand on this general approach in an attempt to identify the *specific* relationship between tropical cyclone intensity and barotropic motion in the Australian region tropical cyclone basin. The physical reasoning behind this suspected relationship is based on the hypothesis that an increase in intensity is generally associated with greater vertical development of the cyclonic vortex, which in turn is advected by an environmental flow of greater depth. A proper and detailed identification of the optimum steering layer will not only be useful for subjective predictions by operational forecasters, but can provide improved initial analysis input for statistical and barotropic track forecast models which initialize on layer-mean wind analyses (such as the operational barotropic model employed in Australia which uses a 1000–100-hPa deep

Corresponding author address: Mr. Christopher S. Velden, SSEC, University of Wisconsin, 1225 West Dayton Street, Madison, WI 53706.

layer-mean). These findings should also contribute to further studies of the environmental influences on tropical cyclone motion in the Australian region, through a more proper identification of the basic flow.

A nondivergent barotropic model is employed in this study to investigate the effects on track forecast errors by varying the initial wind analyses (environmental steering flow) based on current storm intensity. The results will allow for an assessment of the importance of the initial analysis and intensity information in barotropic track forecasting.

2. Data sample

Tropical cyclone "best track" data from Australian region storms are on archive at the Australian Bureau of Meteorology. This data set consists of 6-h information that includes the storm date/time, and observations/estimates of current position, central pressure, speed, and direction. Also on archive are the objective, operational mandatory-level wind analyses over the Australian region for the period 1971 to the present (Mills and Seaman 1990). Input to the nondivergent barotropic track-forecast model utilized in this study (discussed in the next section) is provided from a selection of these individual mandatory-level wind analyses, and mass-weighted layer-means derived from these horizontal analyses (Pike 1985). The selection process was based on subjective reasoning and previous studies (e.g., Dong and Neumann 1986; Pike 1987).

For the present study, 300 cases from 1971–1990 over the Australian region tropical cyclone basin (roughly 0–40°S and 100–170°E; see Fig. 1) were selected that cover a wide, but evenly-distributed range of intensities from depressions to very strong cyclones. The selection process only required each case to have 48 h of subsequent storm track for model forecast verification, and a 24-h separation between cases to help minimize serial correlations. The Australian region basin offers a severe test of environmental steering concepts since it is characterized by relatively strong vertical shear zones, early track recurvatures and poleward movement, and frequent continental influences (Peak and Elsberry 1984). These effects quite often result in nonpersistent, nonclimatological tracks (Holland 1984) and difficult forecasts (Pike and Neumann 1987).

3. Model description

The procedures for analyzing the wind field and predicting the forecast track are: 1) the removal of the tropical cyclone vortex from the initial wind analysis and replacement with the environmental flow; 2) a nondivergent barotropic forecast of the environmental flow field; and 3) a point (storm center) trajectory forecast based on the barotropic forecast of the environmental flow. This methodology was chosen to minimize the variance of the tropical cyclone motion due to the vortex specification and interaction, and to focus

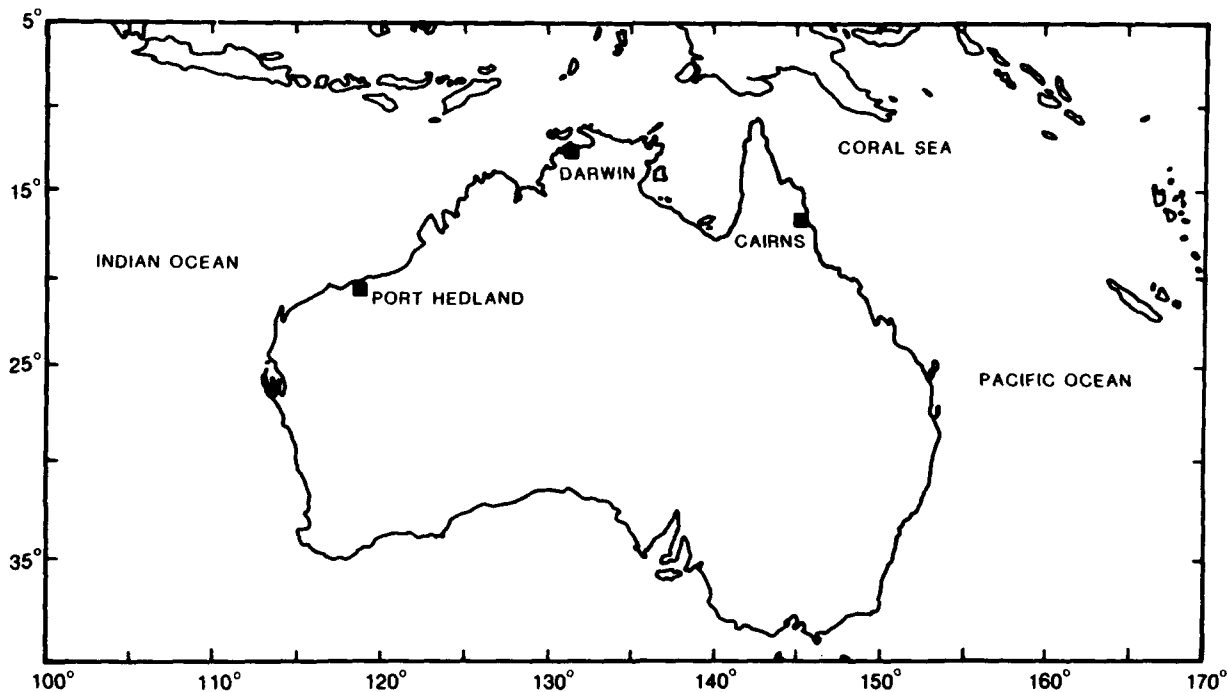


FIG. 1. Australian region tropical cyclone domain.

specifically on the effects of varying the environmental flow field.

The axisymmetric tropical cyclone vortex is removed from the initial objective wind analysis by zeroing out all grid point values within a specified radius of the storm center. This radius is determined from the operationally-analyzed outermost closed isobar. Bi-linear interpolation from surrounding grid point values just outside the specified radius is used to re-assign values to all grid points that were zeroed out. This simple procedure, in effect, approximates the environmental flow over the original vortex region.

The environmental flow is assumed to be governed by the nondivergent barotropic vorticity equation, which expresses conservation of the vertical component of absolute vorticity following parcels on a sphere:

$$\frac{\partial \zeta}{\partial t} + \vec{V} \cdot \vec{\nabla} (\zeta + f) = 0, \quad (1)$$

where \vec{V} is the horizontal, nondivergent wind, ζ is the relative vorticity on a sphere, and f is the Coriolis parameter. Since \vec{V} is nondivergent, we may write its eastward (u) and northward (v) components in terms of a stream function:

$$u = -\frac{\partial \psi}{\partial y}, \quad v = \frac{\partial \psi}{\partial x}. \quad (2)$$

Here, x and y are, respectively, the eastward and northward coordinates along the surface of the sphere. Changing coordinates to latitude (ϕ) and longitude (λ), and making use of (2), the relative vorticity is then:

$$\zeta = \nabla^2 \psi = \frac{1}{r^2 \cos \phi} \frac{\partial}{\partial \phi} \left(\cos \phi \frac{\partial \psi}{\partial \phi} \right) + \frac{1}{r^2 \cos^2 \phi} \frac{\partial^2 \psi}{\partial \lambda^2}, \quad (3)$$

where r is the earth radius, and ∇^2 is the Laplacian operator in spherical coordinates. The streamfunction-vorticity tendency equation becomes

$$\frac{\partial \zeta}{\partial t} = \frac{1}{r^2 \cos \phi} \left[\frac{\partial(\zeta + f)}{\partial \lambda} \frac{\partial \psi}{\partial \phi} - \frac{\partial(\zeta + f)}{\partial \phi} \frac{\partial \psi}{\partial \lambda} \right] = (\nabla^2 - R^{-2}) \frac{\partial \psi}{\partial t}, \quad (4)$$

that is,

$$\frac{\partial \psi}{\partial t} = (\nabla^2 - R^{-2})^{-1} \frac{\partial \zeta}{\partial t} \quad (5)$$

where R is the internal Rossby radius of deformation, which we take to be 1000 km. This additional term is included to take into account the first internal mode. Without this term, Cressman (1958) has shown that there is an unrealistic retrogression of long waves in nondivergent barotropic models.

The model equations are solved using leapfrog time differencing and centered spatial differencing on a lim-

ited-area, latitude-longitude grid located over the Australian region analysis domain (Fig. 1). The latitude and longitude increments are equal and fixed at one degree. Since the model domain is confined to lower latitudes, numerical problems with this finite-difference scheme at higher latitudes (e.g., convergence of the meridians, singularities at the poles) do not arise. The solution procedure is as follows: the vorticity field is calculated from (3). Then the forcing term is computed from (4). Next, the Helmholtz equation (5) is solved for $\partial \psi / \partial t$. Finally, the streamfunction is updated in time.

Because of the limited model domain, it is necessary to specify horizontal boundary conditions for $\partial \psi / \partial t$ when inverting the Laplacian. The simple boundary condition employed in our sensitivity studies is $\partial \psi / \partial t = 0$. This is applied to the two outermost sets of points. In addition, a Rayleigh-type relaxation term is added to (4) for the next three sets of points inward. This term is proportional to $\partial \psi / \partial t$ and is intended to nudge $\partial \psi / \partial t$ towards zero over this region. The coefficient of the term has a maximum value of $2/r^2 \cos \phi \Delta \lambda \Delta \phi$ and decreases linearly to zero in the interior of the domain. Here, $\Delta \lambda$ and $\Delta \phi$ are the longitude and latitude increments, respectively.

The final step is a simple trajectory procedure which follows a point (storm center) in the fluid (environmental flow) during the barotropic model integration (Velden et al. 1984). This step is necessary because of the elimination of the vortex (and associated vorticity center) as described above. The trajectory begins at the specified storm center location, and is calculated after each time step based on the barotropic forecast of the environmental flow.

TABLE 1. Mean track forecast errors (km) from various wind analyses used to initialize the barotropic track forecast model. The number of cases is 300. The lowest MFE for each period is underlined.

	Forecast interval (h)			
	12	24	36	48
<i>Single levels (hPa)</i>				
850	108	211	280	381
700	106	209	272	375
500	111	216	286	389
400	117	226	297	415
<i>Single-level combinations (hPa)</i>				
850, 200	125	239	311	437
850, 500, 200	117	221	293	412
850, 400, 200	118	228	305	427
<i>Layer-means (hPa)</i>				
1000-100	93	193	267	359
850-200	89	189	249	346
850-300	<u>85</u>	183	242	<u>336</u>
850-400	87	<u>182</u>	240	338
850-500	89	186	246	341
700-400	94	197	251	351
700-500	96	202	254	356

TABLE 2. 48-h mean track forecast errors (km) from various layer-mean wind analyses used to initialize the barotropic track forecast model for specified tropical cyclone intensity classes. The total number of cases is 300, which are fairly evenly distributed among intensity classes. The lowest forecast error for each intensity class is underlined.

Intensity class (hPa)	>1005	995-1005	985-995	975-985	965-975	955-965	945-955	935-945	<935
No. of cases	25	25	25	25	50	50	25	25	50
Layer-means (hPa)									
1000-100	389	374	367	364	367	364	347	338	324
850-200	383	365	357	355	348	339	328	326	313
850-300	371	362	355	351	331	332	310	304	302
850-400	343	341	349	344	<u>322</u>	<u>316</u>	334	341	339
850-500	<u>332</u>	<u>331</u>	<u>332</u>	337	332	329	356	360	356
700-400	348	338	347	342	345	341	361	365	368
700-500	342	<u>331</u>	340	346	359	367	372	377	372

This forecast procedure is both simple and economical, and has been employed in previous sensitivity/impact studies (Velden et al. 1984; Velden 1990). It is appropriate for use in our analysis as it provides for a forecast based purely on the specified environmental steering current. The results presented in the next section are based upon 48-h forecasts from this model.

4. Results

We first consider the relative performance of selected single-level wind analyses, single-level combinations (with individual levels given weights determined by regression equations provided by the ERL-Hurricane Research Division), and vertically averaged (mass-weighted) tropospheric layer-means as input to the model for the entire sample, before stratifying by storm intensity. Mean forecast errors (MFEs) for the 300 cases are shown in Table 1. Care must be taken in the interpretation of this table. As we will show later in the text, storms with different intensities move with different flow regimes and inherent forecast difficulty levels. Since we deliberately chose a sample with an evenly-distributed range of intensities, and not a climatological intensity distribution, generalizations about Australian region tropical cyclone steering cannot be gleaned from this particular table. The focus is on the relative differences between the MFEs for a sample with evenly-distributed intensities.

Table 1 shows 12, 24, 36, and 48-h forecasts (km) from the barotropic model initialized with selected wind analyses. Considering first the single-level analyses, the results show that the MFEs for 700 hPa are slightly lower than 850 hPa, moderately lower than 500 hPa, and significantly lower (student-t test 95% significance level will be used throughout the paper) than the 400-hPa MFE. The MFE from the selected single-level combinations are generally higher than the single-level MFE, which suggests that adding upper-tropospheric (outflow region) information is detrimental to approximating the steering current, at least in the context of barotropic track forecasting.

A substantial reduction in MFE occurs when layer-

mean fields are used as input to the model. Overall, the 850-300 and 850-400-hPa layer-means yield the lowest MFE, and are significantly lower than the MFE from the optimum single-level (700 hPa) and the 1000-100-hPa DLM commonly utilized in operational models that incorporate layer-mean wind analyses as input. This supports the findings of previous studies (e.g., Dong and Neumann 1986; Pike 1987) that tropospheric layer-means, as opposed to single-levels, should be used to provide the best approximation to environmental steering. However, at least in the Australian region, the traditional 1000-100-hPa DLM is not the optimal layer. This supports our previous observation and the contention by Holland (1984) that boundary and outflow layer asymmetries do not contribute to the basic current, and may even introduce variance, at least in the context of barotropic environmental steering. [Upper-tropospheric synoptic-scale circulations such as TUTT cells (Sadler 1976, 1978),

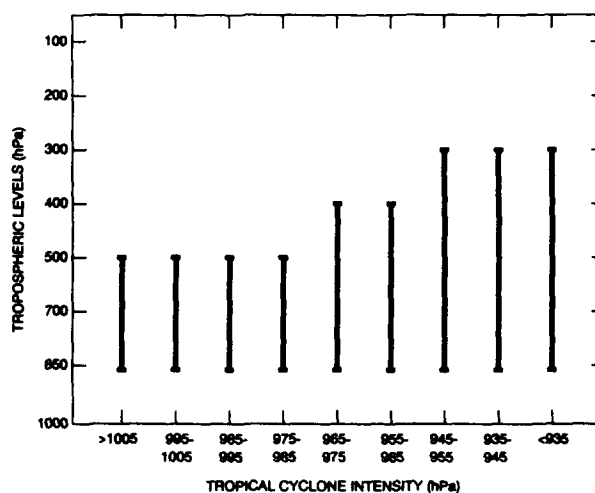


FIG. 2. The relationship between tropical cyclone intensity (MSLP) and the depth of the steering layer in the Australian region. The thick bars indicate the layer-mean wind analysis that provides the optimum 48-h track forecast in each intensity category. (Note: as indicated in Table 2, there was a tie between the 850-500- and 700-500-hPa layer-means for the 995-1005-hPa intensity category).

or mobile, mid-latitude troughs (Velden 1987) can influence the cyclone path, but these baroclinic interactions are not considered here.) Holland (1984) also suggests the general use of the 850–300-hPa layer for approximating the basic current in Australian tropical cyclones. As discussed later, this layer is valid for intense systems, but is not optimum for weaker storms.

Given the results shown in Table 1, only the layer-mean fields are examined further. The MFE differences between the “best” three or four layer-means are quite small, and an optimal layer-mean is not obvious. This is especially true given the evidence presented later in the text that intense storms (in which the 850–300-hPa layer-mean is optimum) exhibit lower overall MFE than weaker storms. It is emphasized that these results should not be interpreted as a general finding for the Australian region basin, since our sample intensities are intentionally evenly-distributed, and not based on climatology.

To investigate the influence of intensity (*defined as the current minimum sea level pressure, MSLP*) on the selection of the optimum steering layer, the sample is stratified into 10-hPa intensity classes shown in Table 2 (while only the 48-h MFEs are shown, similar results were found at other forecast intervals). From Table 2, our objective results seem to confirm intuitive reasoning that the motion of weaker storms is best approximated by shallow layer-means, and intense storms by deep layer-means. Figure 2 graphically represents the relationship between the optimum steering layer (lowest MFE) and intensity. It is clear that a general relationship exists, although due to the somewhat narrow intensity stratification, the differences in MFEs in Table 2 are generally not significant. This may, in part, be due to the variance in the best track intensity estimates that were derived almost solely from satellite techniques that were evolving during the period of this study (Holland 1981).

It is suggested from Fig. 2 that a re-stratification into three broader intensity classes (>975, 955–975, <955 hPa) would adequately represent the steering/intensity relationship. This broader intensity stratification will also reduce the likelihood of variance due to unrepresentative intensity estimates. The MFEs (48-h) are presented in Table 3, and show that the 850–500-hPa

TABLE 3. As in Table 2, except for different intensity classes.

Intensity class (hPa)	>975	955–975	<955
No. of cases	100	100	100
Layer-means (hPa)			
1000–100	374	365	336
850–200	365	344	322
850–300	360	332	305
850–400	345	318	338
850–500	333	330	357
700–400	344	343	365
700–500	340	356	374

TABLE 4. A summary of the variability of the results in Table 3. The numbers indicate how many times each particular layer-mean yielded the best (worst) forecast for each intensity category.

Intensity class (hPa)	>975	955–975	<955
No. of cases	100	100	100
Layer-means (hPa)			
1000–100	6 (32)	8 (16)	16 (8)
850–200	5 (27)	10 (8)	23 (5)
850–300	6 (17)	20 (9)	34 (2)
850–400	21 (8)	31 (4)	17 (12)
850–500	36 (4)	13 (11)	3 (24)
700–400	12 (7)	14 (20)	4 (22)
700–500	14 (5)	4 (32)	3 (27)

layer is optimal for less intense storms with central pressures higher than 975 hPa; the 850–400-hPa layer is optimal for storms with central pressures between 955 and 975 hPa; and the 850–300-hPa layer is optimal for the most intense storms with central pressures lower than 955 hPa. The 850–200-hPa layer provided the lowest MFE for storms with central pressures lower than 925 hPa. However, the very small number of cases prevented this result from being significant, and is not shown. Differences in the MFE between the layer with the lowest and next lowest values are significant for each intensity category. Table 4 presents a summary of the variability of these results. Shown for each layer-mean are the number of forecasts that yielded the best (and worst) 48-h position errors relative to the other layer-means, for each intensity category. The highest number of optimal forecasts in each intensity category corresponds to the layer-mean with the lowest MFE shown in Table 3, suggesting a strong degree of consistency in the results.

Similar results are also found with the 12-, 24-, and 36-h MFE (not shown), and specifically identify the greater depth of the optimal deep-layer environmental steering relative to increasing tropical cyclone intensity in the Australian region. This information should be very useful to operational forecasters for subjective purposes, and can be employed to more appropriately initialize operational statistical and barotropic numerical track forecast models.

To illustrate further the varying flow regimes and resulting track forecasts depending on layer-mean depth and storm intensity, two examples of individual cases are presented. These examples were deliberately chosen to show a typical case, and a dramatic one. The first case involves a weak storm and shows the typical differences in track forecasts that occur depending on which layer-mean wind analysis is used to initialize the model. The second case highlights a strong storm, and shows the dramatic differences in track forecasts that can occur.

a. Tropical cyclone Lena (1983)

Lena developed from a weak tropical low on 1 April and initially moved southwestward (Fig. 3). The storm

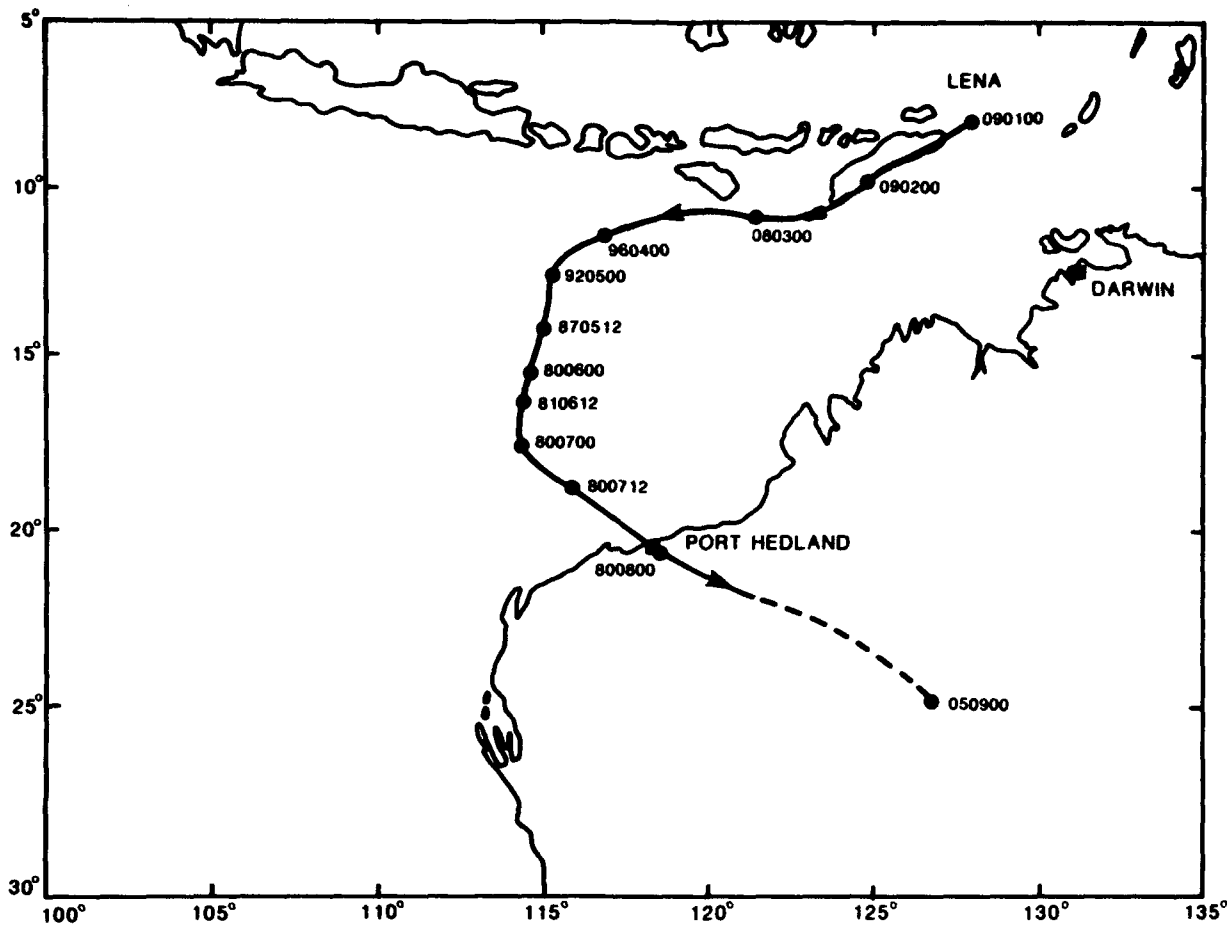


FIG. 3. Track of tropical cyclone Lena during April 1983. The numbers indicate MSLP (87 = 987 hPa), date (01 = 1 April) and time (12 = 1200 UTC), respectively.

then tracked in a westerly direction until 4 April, at which time it reached tropical cyclone status with an estimated central pressure of 994 hPa. Lena then turned southward and deepened to 980 hPa before recurving on 7 April and moving rapidly to the southeast, crossing the Australian coastline near 0000 UTC 8 April. Throughout its lifetime, Lena was a relatively weak system.

To show the impact of properly initializing the barotropic forecast model with a shallow layer-mean wind analysis in a weak cyclone event (as found in our results above), 48-h track forecasts from 1200 UTC 5 April initialized with the 850–500-, 850–300-, and 1000–100-hPa layer-mean wind analyses are presented. The forecast tracks are shown in Fig. 4, while the track forecast errors are given in Table 5. Although the forecast track differences in this case are not dramatic, the shallower layer-mean clearly yields the best results. The track forecast errors of the model initialized with the 850–500-hPa layer-mean are 20–30% lower than with the 1000–100-hPa layer-mean, and illustrate the fact that the motion of this relatively weak cyclone is best ap-

proximated by the lower-tropospheric flow, which in this case has more of a component towards the west than its deep-layer counterpart.

It should be noted that a considerable track forecast error still exists even with the use of the “optimal” 850–500-hPa layer-mean initial analysis. While we considered a reasonable number of layer-mean combinations, it is possible that in some individual cases such as this one, the optimal steering level or layer-mean is one we did not consider (e.g., perhaps in this case the 850–700-hPa layer-mean would be “optimal”). The forecast errors could also be due to analysis uncertainties, model errors, and the fact that we are not considering the beta effect. However, the point is clear in this case and in other more dramatic cases we examined, that in general the weaker intensity systems are steered by the lower-tropospheric flow identified in this study as the 850–500-hPa layer-mean wind.

b. Tropical cyclone Kerry (1979)

The second case involves a very intense storm which occurred during February–March 1979, with an aircraft

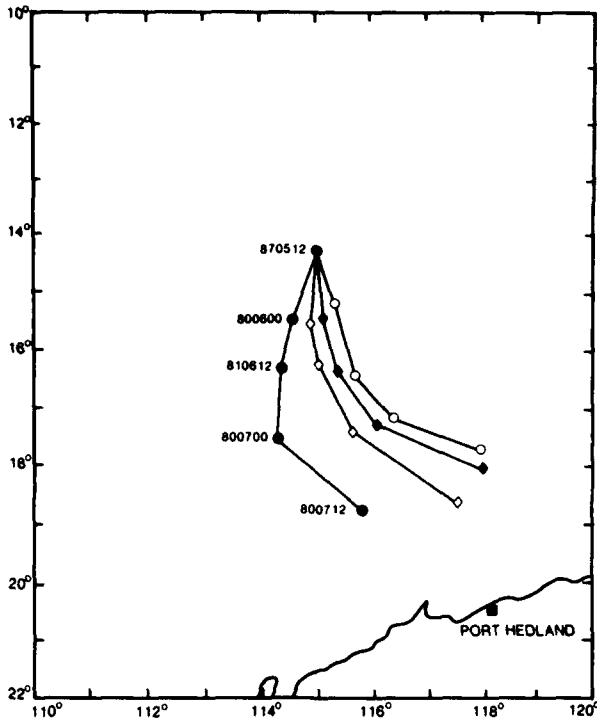


FIG. 4. 48-h track forecasts initialized at 1200 UTC 5 April, along with verifying track for Lena (●--●). Forecasts were initialized with the 850-500- (◇--◇), 850-300- (◆--◆), and 1000-100- (○--○) hPa layer-mean analyses.

recorded sustained wind speed of 140 kt being one of the strongest winds ever observed from an Australian tropical cyclone. Kerry's track was a very long one, and is most notable for its erratic behavior, as evidenced in Fig. 5. By 15 February, as Kerry entered the Australian region, it was already classified as a severe tropical cyclone. The central pressure decreased to 943 hPa on 19 February. In the period of 19-26 February, Kerry moved in a large loop before heading westward towards the eastern Australian coast. In the next week or so, Kerry persisted near the coast before finally accelerating to the southeast and weakening.

Track forecasts were initialized at 1200 UTC 18 February, near the time when Kerry was most intense. As in the previous case, the forecasts from the 850-500-, 850-300-, and 1000-100-hPa initial wind analyses are compared both graphically (Fig. 6), and quantitatively (Table 6). In contrast to the weak case presented above, the best forecast in this case results when the model is initialized with a deep-layer mean (850-300 hPa). This illustrates an example of an intense system which is characterized by a well-developed (vertically) vortex which moves with a deeper flow. Note, however, that the traditionally-utilized 1000-100-hPa DLM results in an inferior forecast, indicating possible negative effects on approximating the vortex motion from the inclusion of the inflow and outflow regions, as discussed earlier. The areal-averaged upper-

tropospheric flow at and above 200 hPa at this time was a weak southeasterly, while the 1000-hPa flow was from the east, resulting in the northwest shift of the 1000-100-hPa track relative to the 850-300-hPa track.

It is interesting to note from Table 3 that the optimum layer MFEs for the intense storms (<955 hPa) are significantly lower than the optimum layer MFE for the weaker storms (>975 hPa). This finding is consistent with the results of Dong and Neumann (1986) for easterly moving Atlantic hurricanes versus tropical storms. This could be physically related to the more persistent nature of deep-layer steering associated with the more intense storms, but could also be attributed to increased initial positioning errors associated with weaker systems (DeMaria et al. 1990).

The overall MFE when the optimal layer (based on the three intensity categories) is used in each individual case (dependent sample) to initialize the model is shown in Table 7. This method results in a significant reduction in MFE (up to 12% at 48 h) over that of a fixed-layer (1000-100 hPa) initialization that does not include intensity information (i.e., the current operational procedure at the Bureau of Meteorology in Australia). This is quite a remarkable improvement given that the experiment involves only a modest change in the initial analyses provided to the forecast model.

While relative comparisons are the main focus of this paper, the forecast results using the optimal layer are also compared, in an absolute sense, to persistence and the official track forecasts from these 300 cases to assess the competitiveness of this numerical guidance (Table 7). It is shown that the MFE are much lower than persistence, and quite competitive with the official forecasts (derived from operational storm positions). This is despite the fact that the model is governed solely by environmental steering, and does not include the contributions to motion from linear and nonlinear effects of vortex propagation.

5. Discussion

The results show that the initialization of a barotropic tropical cyclone track forecast model with a variable-depth wind analysis that best approximates the

TABLE 5. Track forecast position errors (km) for weak tropical cyclone Lena (987 hPa) from 1200 UTC 5 April 1983. A comparison is made between model forecasts initialized with the 850-500-, 850-300-, and 1000-100-hPa layer-means.

	Forecast interval (h)			
	12	24	36	48
<i>Layer-mean (hPa)</i>				
850-500	47	106	134	202
850-300	63	129	171	249
1000-100	71	147	189	268

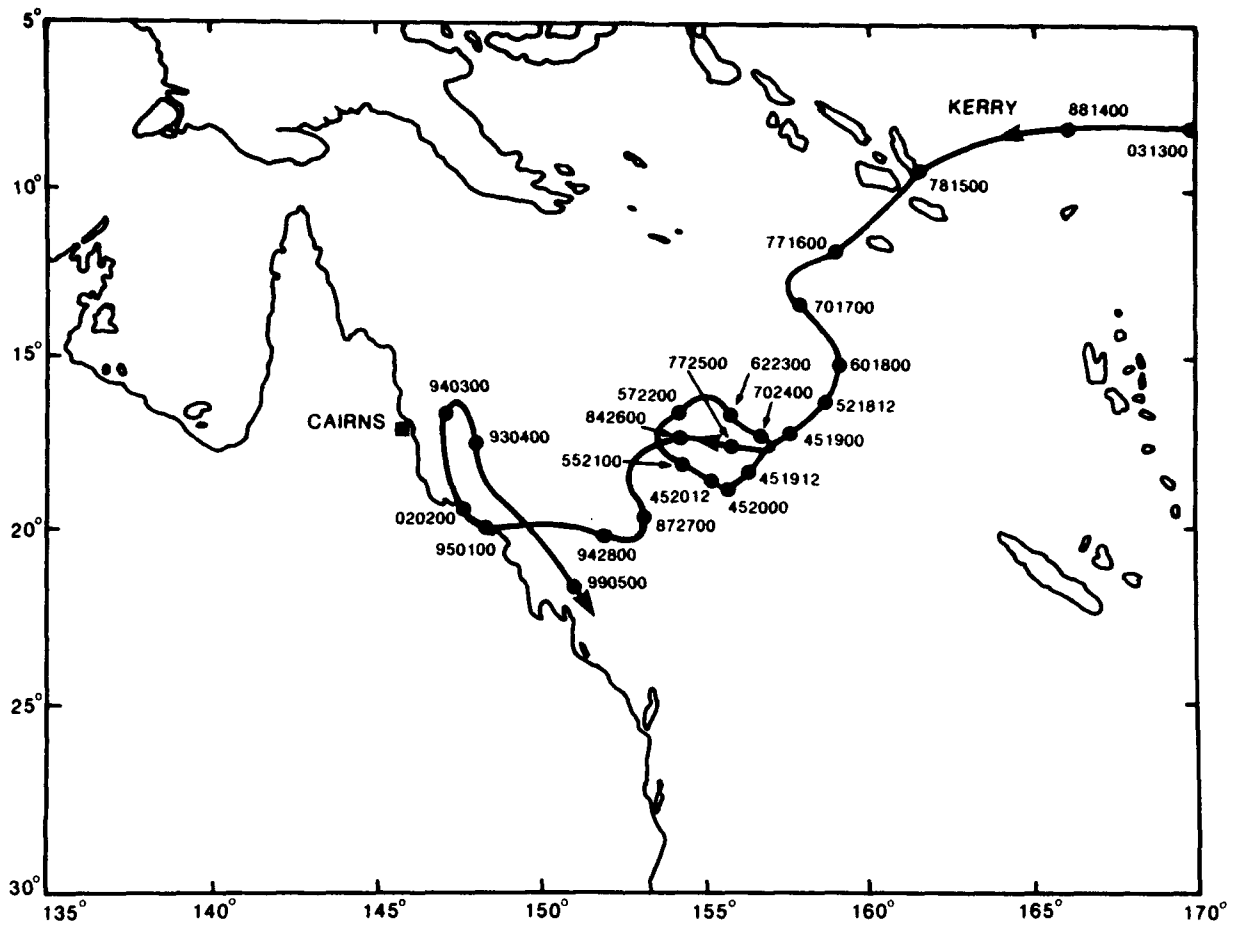


FIG. 5. Track of tropical cyclone Kerry during February and March of 1979. The numbers are as explained in Fig. 3.

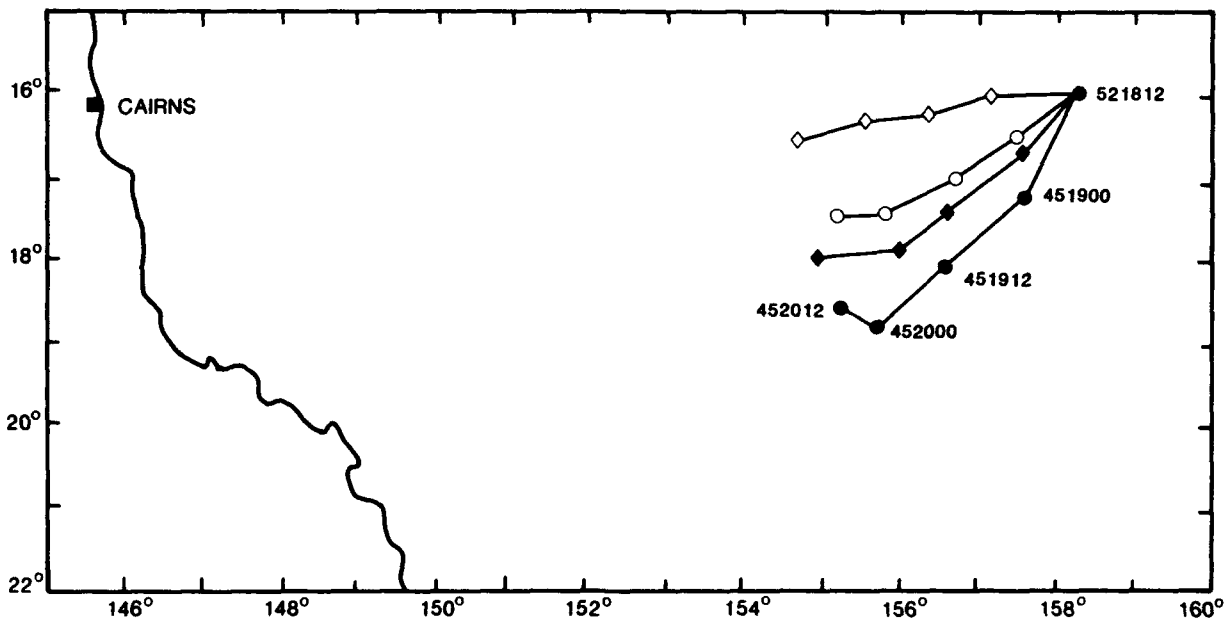


FIG. 6. 48-h track forecasts initialized at 1200 UTC 18 February, along with verifying track for Kerry (●--●). Forecasts were initialized with the 850-500- (◇--◇), 850-300- (◆--◆), and 1000-100- (○--○) hPa layer-mean analyses.

environmental steering can significantly reduce the MFE relative to a "fixed-depth" analysis. The current operational schemes at the Australian Bureau of Meteorology utilize a 1000–100-hPa DLM in all forecast situations regardless of intensity, as does the operational SANBAR barotropic model (Sanders et al. 1975) in the Atlantic and eastern North Pacific basins. This study shows that the selection of the optimum wind analysis is dependent on storm intensity, with tropospheric layer-means outperforming single-level analyses. The model MFE for weaker systems (>975 hPa) are minimized using the 850–500-hPa layer-mean, while the optimal wind analysis for very intense storms (<955 hPa) is the 850–300-hPa layer-mean.

These findings for the Australian region support the intuitive concept that the depth of the environmental steering increases with tropical cyclone intensity. The fact that a strong relationship was found in this tropical cyclone basin, which is characterized by relatively weak environmental flow regimes and erratic tracks, suggests that the basic concept would apply in other basins. In fact, Dong and Neumann (1986) found similar results in the Atlantic, although their stratifications and optimal layer-means differed somewhat.

There are physical and environmental factors which can affect the basic relationships and optimum steering layer-means. Some of these (storm latitude, intensity tendency, season, specific area of development, and environmental easterlies versus westerlies regimes) will be a subject of future work, and can be incorporated into the operational schemes. There are other situations that could lead to deviations from the above results in individual storm events. Initial analysis and intensity estimate uncertainties (Holland 1981), land effects (Holland 1984), and strongly sheared environments (Chan and Gray 1982); or subtropical "hybrid" developments might require special considerations.

The tropical cyclone vortex was eliminated from the flow field in our study to isolate the effects on forecast motion exclusively by the environmental flow. Thus, we have not considered the potential effects of the variable-depth analyses on the component of tropical cyclone motion associated with vortex propagation (Chan and Williams 1987; Fiorino and Elsberry 1989). However, these findings may be important to studies

TABLE 6. Track forecast position errors (km) for strong tropical cyclone Kerry (945 hPa) from 1200 UTC 18 February 1979. A comparison is made between model forecasts initialized with the 850–500-, 850–300-, and 1000–100-hPa layer-means.

	Forecast interval (h)			
	12	24	36	48
<i>Layer-mean (hPa)</i>				
850–500	127	210	246	238
850–300	59	76	105	82
1000–100	86	112	137	121

TABLE 7. A comparison of mean track forecast errors (km) by different methods for the homogeneous sample of 300 cases. From the barotropic model forecasts, the operational layer-mean is the 1000–100-hPa DLM (fixed for all cases), and the optimum layer-mean (variable in each case) is based on the intensity stratification of Table 3. The official forecasts were made from operational initial positions and all others from best track position.

<i>Method</i>	Forecast interval (h)			
	12	24	36	48
Persistence	87	203	358	505
Official	96	201	280	382
Operational layer-mean	93	193	267	359
Optimum layer-mean	81	172	230	319

of the interaction of the vortex with the environment by more accurately defining the basic flow.

From an operational standpoint, the performance of the barotropic track forecast model with the inclusion of the intensity information should boost the confidence Australian forecasters have in the ability of these simple models to predict tropical cyclone tracks. There has been a tendency to overlook these models with the recent influx of sophisticated schemes and dynamic models. Certainly, the sheer simplicity of the model dynamics will explain much of the forecast position error in barotropic track forecasting. However, it is suggested from these results that a significant part of the forecast error can be attributed simply to the improper specification of the depth of the wind analysis used to initialize these models.

These results also suggest that intensity prediction could be very important to barotropic track forecasting. The plausibility exists of incorporating prognostic intensity information into the barotropic track forecast model (to determine if the optimum layer changes during the integration). Any additional reduction in track MFE will of course be dependent upon the ability to accurately forecast intensity. Current operational methods show limited skill, however, preliminary results of experimental schemes being tested at the Australian Bureau of Meteorology are showing promise (Leslie et al. 1990). The possibility of incorporating this prognostic intensity information into the track forecast model described here is being investigated.

Acknowledgments. The authors would like to thank John McBride and Greg Holland for useful discussions, David Pike for drafting and programming assistance, and Laura Beckett for preparing the manuscript. This study was partially funded by ONR grant N00014-88-K-0711.

REFERENCES

- Chan, J. C.-L., and W. M. Gray, 1982: Tropical cyclone movement and surrounding flow relationships. *Mon. Wea. Rev.*, **110**, 1354–1374.

- , and R. T. Williams, 1987: Analytical and numerical studies of the beta-effect in tropical cyclone motion. Part 1. Zero mean flow. *J. Atmos. Sci.*, **44**, 1257–1264.
- Cressman, G. P., 1958: Barotropic divergence and very long atmospheric waves. *Mon. Wea. Rev.*, **86**, 293–297.
- DeMaria, M., M. B. Lawrence and J. T. Kroll: An error analysis of Atlantic tropical cyclone track guidance models. *Wea. Forecasting*, **5**, 47–61.
- Dong, K., and C. J. Neumann, 1986: The relationship between tropical cyclone motion and environmental geostrophic flows. *Mon. Wea. Rev.*, **114**, 115–122.
- Elsberry, R. L., W. M. Frank, G. J. Holland, J. D. Jarrell and R. L. Southern, 1987: A global view of tropical cyclones. Copies available from R. L. Elsberry, Dept. of Meteorology, Naval Postgrad. School, Monterey, California.
- Fiorino, M., and R. L. Elsberry, 1989: Some aspects of vortex structure related to tropical cyclone motion. *J. Atmos. Sci.*, **46**, 975–990.
- Holland, G. J., 1981: On the quality of the Australian tropical cyclone data base. *Aust. Meteor. Mag.*, **29**, 169–181.
- , 1984: Tropical cyclones in the Australian/Southwest Pacific region. *Aust. Meteor. Mag.*, **32**, 1–33.
- Leslie, L. M., G. D. Hess, G. J. Holland and R. P. Morrison, 1991: Forecasting intensity changes in tropical cyclones using Markov chain techniques. Submitted to *Wea. Forecasting*.
- Mills, G. A., and R. S. Seaman, 1990: The BMRC regional data assimilation system. *Mon. Wea. Rev.*, **118**, 1211–1237.
- Peak, J. E., and R. L. Elsberry, 1984: Dynamical-statistical model forecasts of Southern Hemisphere tropical cyclones. *Mon. Wea. Rev.*, **112**, 717–724.
- Pike, A. C., 1985: Geopotential heights and thicknesses as predictors of Atlantic tropical cyclone motion and intensity. *Mon. Wea. Rev.*, **113**, 931–939.
- , 1987: A comparison of wind components and geopotential heights as statistical predictors of tropical cyclone motion. *Ext. Abst. 17th Conf. Hurr. and Trop. Meteor.*, Miami, Amer. Meteor. Soc., 101–103.
- , and C. J. Neumann, 1987: The variation of track forecast difficulty among tropical cyclone basins. *Wea. Forecasting*, **2**, 237–241.
- Sadler, J. C., 1976: A role of the tropical upper tropospheric trough in early season typhoon development. *Mon. Wea. Rev.*, **104**, 1266–1278.
- , 1978: Mid-season typhoon development and intensity changes and the tropical upper tropospheric trough. *Mon. Wea. Rev.*, **106**, 1137–1152.
- Sanders, F., A. C. Pike and J. P. Gaertner, 1975: A barotropic model for operational prediction of tracks of tropical storms. *J. Appl. Meteor.*, **14**, 265–280.
- Simpson, R. H., 1971: The decision process in hurricane forecasting. NOAA Tech. Memo. NWS SR-53, 30 pp. Available from U.S. Dept. of Commerce, Washington DC, 20233.
- Velden, C. S., 1987: Satellite observations of hurricane Elena (1985) using the VAS 6.7 micron water-vapor channel. *Bull. Amer. Meteor. Soc.*, **68**, 210–215.
- , 1990: The impact of satellite-derived winds on hurricane analysis and track forecasting. *Ext. Abst. 5th Conf. Satellite Meteor. and Ocean.*, London, England, Amer. Meteor. Soc., 215–219.
- , W. L. Smith and M. Mayfield, 1984: Application of VAS and TOVS to tropical cyclones. *Bull. Amer. Meteor. Soc.*, **65**, 1059–1067.

PHYSICAL RETRIEVAL OF TYPHOON STRUCTURE USING PASSIVE MICROWAVE OBSERVATIONS

Robert T. Merrill

Cooperative Institute for Meteorological Satellite Studies
University of Wisconsin, Madison WI 53706

1. INTRODUCTION

Microwave radiometers in the 55 GHz O₂ band can detect changes in air temperature even through clouds and snow. An obvious application is measuring the strength of warm cores of tropical cyclones. Because the hydrostatic approximation is valid for tropical cyclones, the three-dimensional temperature structure determines the sea level pressure distribution. The minimum sea level pressure (MSLP) or its deviation from the environmental pressure (ΔP) are useful indices of a tropical cyclone's intensity.

It is therefore possible to estimate tropical cyclone intensity if one can retrieve the three-dimensional temperature anomaly from the observed brightness temperatures (T_b) at various scan line and element (i, j) locations and frequencies (k). Neglecting scattering by precipitation (minimal above the melting level) and surface emission (minimal for upper-tropospheric channels),

$$T_{B_{i,j,k}} = \int_{VOL} W_k(z) T(x,y,z) F_{i,j}(x,y) dVOL \quad (1)$$

where $W_k(z)$ is the weighting function for channel k , $T(x,y,z)$ is the three dimensional temperature structure, and $F_{i,j}(x,y)$ is the projection of the antenna pattern at scan coordinate (i, j) onto the Earth's surface.

In principle, (1) can be inverted for a set of $T_{B_{i,j,k}}$ to obtain $T(x,y,z)$ directly. This is a generalization of the classical sounding retrieval problem (Rodgers 1976) to include the interaction between $T(x,y,z)$ and $F_{i,j}(x,y)$. This horizontal structure must be modeled explicitly because the antenna "footprint" and warm anomaly are of similar sizes (Fig. 1). The maximum brightness temperature seen by the radiometer is less than would be measured if the horizontal resolution was less than the eye diameter.

The complexity of (1) motivates the replacement of part or all of the solution with regression. Velden et al. (1991) develops statistical relationships for ΔP (central pressure anomaly) for western North Pacific tropical cyclones using measurements from the Microwave Sounding Unit (MSU) aboard the NOAA series polar orbiters. A purely statistical method relates ΔP

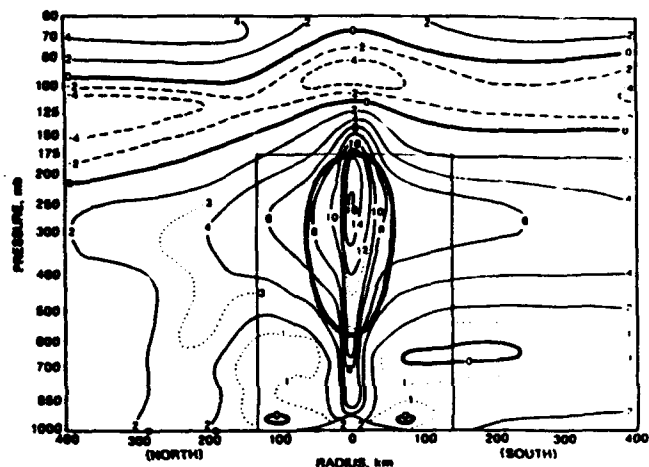


Figure 1. Cross section in radius and height of temperature anomalies in Hurricane Inez (1966) based on rawinsondes (located at black dots on abscissa), aircraft flights in the low, middle, and upper troposphere (within rectangular outline, Hawkins and Imbombo 1976), and the mean hurricane stratospheric structure from Koteswaram (1967). Anomalies are relative to the mean annual sounding for the West Indies (Jordan 1958). If Inez were viewed at nadir and centered in an antenna footprint, roughly half of the energy received by MSU Channel 3 would come from inside the oval.

measured by aircraft to the difference in Channel 3 brightness temperature between the measurement nearest the center and an environmental mean ($T_{bc} - T_{benv}$); to ΔP . (Channel 3 is chosen because its weighting function peaks in the upper troposphere where the warm core is strongest.) A hybrid method applies a physical sounding retrieval algorithm (Smith 1970) to the four MSU channels; ΔP is then related statistically to the 250 hPa temperature difference ($T_o - T_{env}$)₂₅₀.

The present research is motivated by the desire to use SSM/T (DMSP series Special Sensor Microwave/Temperature) data to estimate the intensity of western North Pacific tropical cyclones. Velden et al.'s (1991) results cannot be used because they are based on MSU data with a horizontal resolution of 110 km at nadir, while the SSM/T

resolution is 180 km. Neither can a new statistical relationship be made specifically for SSM/T, because SSM/T archiving began after aircraft reconnaissance (source of ΔP ground truth) was discontinued in 1987.

What is needed is an algorithm which accounts for satellite-dependent factors (antenna pattern and weighting function) without the need for ground truth and produces an estimate of warm core strength which does not depend upon the instrument. The difference in weighting functions can be accounted for by using a sounding retrieval algorithm. This extended abstract describes a feasibility study of the other half of the problem -- correcting for antenna resolution effects using a physical retrieval approach.

2. HORIZONTAL STRUCTURE RETRIEVAL CONCEPT

If the horizontal structure of the warm anomaly does not vary significantly with height over the depth of $W_k(z)$, we can write $T(x,y,z)$ as

$$T(x,y,z) = T_0(z) + \Delta T_{max}(z)T^*(x,y) \quad (2)$$

where $T_0(z)$ is the environmental sounding, $\Delta T_{max}(z)$ is the maximum anomaly (eye) sounding, and $T^*(x,y)$ is the nondimensionalized horizontal anomaly structure. The origin is assigned to the tropical cyclone center and $T^*(0,0)=1$. Assuming the weighting functions do not vary across the tropical cyclone, we can substitute (2) into (1)

$$T_{B1,j,k}^{obs} = \int_0^{\infty} \int_{AREA} \{ W_k(z) F_{1,j}(x,y) [T_0(z) + \Delta T_{max}(z)T^*(x,y)] \} dAREA dz \quad (3)$$

Since $\int_{AREA} F(x,y) dAREA = 1$, integrating (3) yields

$$T_{B1,j,k}^{obs} = T_{B0,k} + \Delta T_{Bk} \int_{AREA} F_{1,j}(x,y) T^*(x,y) dAREA \quad (4)$$

The brightness temperatures on the right hand side result from the vertical integration of the environmental and maximum (eye) anomaly temperature structures, respectively, with the channel k weighting function.

The use of an observed T_B anomaly $(T_{B0} - T_{Benv})_k$ as an estimate of ΔT_{Bk} (see Introduction) implicitly assumes that $T^*(x,y)=1$ over the antenna "footprint" $F_{1,j}(x,y)$. The area integral is therefore overestimated by a factor which varies directly with the size of the antenna footprint. $(T_{B0} - T_{Benv})_k$ therefore underestimates ΔT_{Bk} so the statistical regression between ΔT_{Bk} and ΔP compensates by adjusting the coefficient on ΔT_{Bk} upward to account for the horizontal resolution effect for the average $T^*(x,y)$.

The goal of the horizontal physical retrieval algorithm is to determine the eye anomaly $\Delta T_{Bmax}(z)$ and anomaly structure $T^*(x,y)$ which best reproduce a set of observed $T_{B1,j,k}$ across the warm core. The retrieval is performed by inverting

$$T_{B1,j,k}^{obs} = \int_{AREA} F_{1,j}(x,y) T_{Bk}(x,y) dAREA. \quad (5)$$

The warm core structure $T_{Bk}(x,y)$ seen by a radiometer with very high horizontal resolution is modeled as

$$T_{Bk}(x,y) = T_{B0,k} + \Delta T_{Bk} [1 - \exp(-\frac{\alpha}{r})^\beta] + T_{Bkx} + T_{Byy} \quad (6)$$

where

$$r = (x^2 + y^2)^{1/2}.$$

Parameters α and β define the size and shape of the warm anomaly, respectively. T_{Bk} and T_{By} model a uniform environmental thermal gradient. Holland (1980) used the axisymmetric form of this function to fit a variety of tropical cyclone surface pressure distributions. Eq. (6) has been tested for the present application by fitting it to 11 radial temperature profiles from research aircraft flights in Atlantic hurricanes at 180-240 hPa (Shea and Gray 1973).

Parameters $T_{B0,k}$, ΔT_{Bk} , α , β , T_{Bk} , and T_{By} constitute a "structure vector" X , which may be retrieved using the iterative solution of Rodgers (1976):

$$X_{m+1} = X_0 + S_{xx} K_m^T (K_m S_{xx} K_m^T + S_{yy})^{-1} [Y_0 - Y_m - K_m (X_0 - X_m)] \quad (7)$$

where

X_{m+1} - iteration $m+1$ of structure vector

X_0 - "Guess" values of X ,

S_{xx} - Covariance matrix of X ,

Y_0 - Observation vector containing all $T_{B1,j,k}^{obs}$.

S_{yy} - Covariance matrix of observation errors,

Y_m - Predicted observation vector, given by $\int_{AREA} F_{1,j}(x,y) T_{Bk}(X_m, x,y) dAREA$, and

$K_m = [\frac{\partial Y_m}{\partial X_m}]$, evaluated using one-sided finite differences.

3. RESULTS OF HORIZONTAL RETRIEVAL FEASIBILITY TEST

The feasibility of the horizontal physical retrieval is examined by applying it to 77 cases¹ from the western North Pacific MSU set of Velden et al. (1991) and retrieving a brightness temperature structure for Channel 3 $T_{B3}(x,y)$. The algorithm seeks a $T_{B3}(x,y)$ structure which fits the observations without being "unreasonable" (where "reason" is specified by X_0 and S_{xx}). X_0 and S_{xx} for the test are estimated by fitting (6) to aircraft data, followed by some experimentation in which adjustments were made to the mean value of ΔT_{B3} , the standard deviation of α , and the mean of α for those cases in which no eye was reported by reconnaissance (about one-third of the total). These values are summarized in Table 1. For the first iteration ($m=0$), $X_m=X_0$. Eq. (7) is then

¹Five of the original 82 cases could not be processed with the new software.

evaluated repeatedly until the solution for ΔT_{B3} changes by less than 0.5 °K among three successive iterations (4-5 iterations are typically required for convergence). Fig. 2 shows an example of data selection and the retrieved thermal structure.

A quadratic regression equation for ΔP is then fitted to ΔT_{B3} and compared with equations based on $(T_{Bc}-T_{B_{env}})_3$ (pure statistical) and $(T_c-T_{env})_{250}$ (hybrid physical-statistical using a sounding retrieval). The results are shown in Table 2. The regressions based on a retrieved quantity ($(T_c-T_{env})_{250}$ or ΔT_{B3}) are slightly superior to that based on raw brightness temperatures ($(T_{Bc}-T_{B_{env}})_3$). As expected, the coefficient on ΔT_{B3} is smaller than that on $(T_{Bc}-T_{B_{env}})_3$, indicating that the warm anomaly is being more fully resolved.

Eye radii from aircraft will not be available in operational applications. It should be possible to use remote measurements of eye size from visible, infrared, or microwave (SSM/I) imagery instead. The value of this ancillary data is seen by rerunning the physical retrieval with the sample mean eye radius as the guess for all cases; the RMS error on ΔP increases from 15.3 hPa to 16.3 hPa, which is only slightly better than raw radiances (Table 2). However, the physical retrieval still largely serves its purpose if it can correct for antenna differences between MSU to SSM/T, even if it does not improve on raw radiances for any particular instrument.

Table 1. Means and standard deviations for the constraint ("guess") values of the free parameters on the brightness temperature structure modeled by Eq. 6.

QUANTITY	MEAN	STD. DEV.
ΔT_{B3}	5.6 °K	15 °K
$B_{e,3}$	Avg. of outer four observed values, minus 0.5 °K.	1 °K
α	Eye radius from A/G reconnaissance, OR 30 km	0.5 α
β	1	0.5
B_x	0	1 °K/1000 km
B_y	0	1 °K/1000 km

4. SUMMARY AND FUTURE PLANS

The above results demonstrate the overall feasibility of the horizontal physical structure retrieval. As stated in the Introduction, the goals of this study are to be able to use SSM/T to estimate tropical cyclone intensity. The horizontal physical retrieval is an effort to correct for resolution differences between MSU and SSM/T antennas to allow development of a satellite-independent regression relationship for ΔP as a function of retrieved warm core strength.

The ability of the horizontal retrieval to correct for resolution differences between satellites remains to be tested. A preliminary test will be made by using the retrieved structure vector \mathbf{X} and the SSM/T antenna pattern to simulate SSM/T data; the simulated SSM/T data will then be perturbed with simulated noise and used to generate a new retrieval. The values of ΔT_B resulting from the actual MSU-3 and simulated SSM/T data should be similar. The same approach can be used

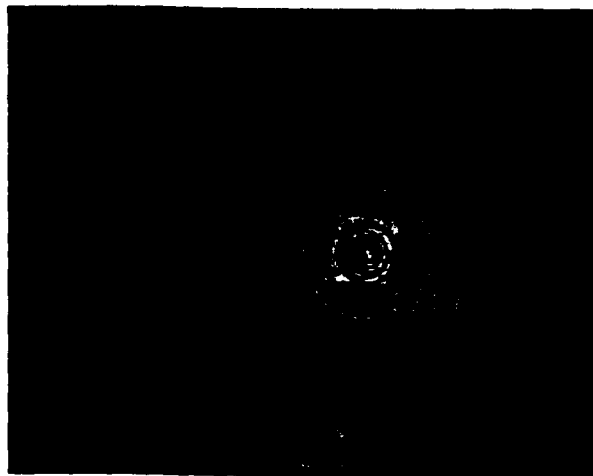


Figure 2. Horizontal physical structure retrieval for Super-Typhoon Forrest, 18 UT 26 Sept. 1983. White areas are warm in the MSU-3 imagery. The ellipses are the half-power footprints of the MSU-3 measurements used. The dashed white contours define the guess temperature structure, and the solid black contours are the retrieved structure. ΔT_{B3} is 5.6 °K in the guess and 19.2 °K in the retrieval.

Table 2. Quadratic statistical relationships for ΔP (central pressure anomaly) using the 77 case sample of western North Pacific tropical cyclones. The $\Delta T_{B3}(AE)$ results are obtained using aircraft measurements of eye radius as a guess for α . $\Delta T_{B3}(ME)$ is obtained when the sample mean eye radius is used for all cases.

Predictor	Equation	Std. Error
(x)	$\Delta P = F(x)$	(hPa)
$(T_{Bc}-T_{B_{env}})_3$	$9.9 + 26.2x - 2.2x^2$	16.6
$(T_c-T_{env})_{250}$	$1.4 + 14.1x - .52x^2$	15.0
$\Delta T_{B3}(AE)$	$9.3 + 7.6x - .19x^2$	15.3
$\Delta T_{B3}(ME)$	$10.8 + 7.7x - .17x^2$	16.3

to test the retrieval for the "next-generation" microwave radiometers: AMSU (Advanced Microwave Sounding Unit) and the SSM/T2, which feature horizontal resolution of order 50 km. Once the scan geometry and navigation for the SSM/T have been added to the retrieval algorithm, it should then be possible to run the horizontal retrieval for both MSU-3 and an upper-tropospheric SSM/T channel. As with the simulation, the retrieved ΔT_B for upper tropospheric channels from different instruments should be similar.

The optimal solution is to apply both horizontal and vertical retrievals in succession and recover an eye temperature anomaly sounding $\Delta T_{max}(z)$ from which ΔP could be computed directly. Considerable difficulties are expected with this approach, but if the reductions in standard error due to the sounding retrieval and horizontal retrieval are largely independent, the use of both should result in improved performance of the regression equation, as well as retaining portability from MSU to SSM/T.

5. ACKNOWLEDGEMENTS.

This work was supported under AFGL Contract #00014-88-K-0711, administered through the Office of Naval Research.

6. REFERENCES

- Hawkins, H. F. and S. M. Imbembo 1976: The structure of a small, intense hurricane: Inez 1966. *Mon. Wea. Rev.* 104, 418-442.
- Holland, G. J. 1980: An analytic model of the wind and pressure profiles in hurricanes. *Mon. Wea. Rev.*, 108, 1212-1218.
- Koteswaram, P. 1967: On the structure of hurricanes in the upper troposphere and lower stratosphere. *Mon. Wea. Rev.*, 95, 541-564.
- Jordan, C. L. 1958: Mean soundings for the West Indies area. *J. Meteor.*, 15, 91-97.
- Shea, D. J. and W. M. Gray 1973: The hurricane's inner core region, I: Symmetric and asymmetric structure. *J. Atmos. Sci.*, 30, 1544-1564.
- Smith, W. L. 1970: Iterative solution of the radiative transfer equation for temperature and absorbing gas profiles of an atmosphere. *Appl. Optics*, 9, 1993-1999.
- Velden, C. S., B. M. Goodman, and R. T. Merrill, 1991: Western North Pacific tropical cyclone intensity estimation from NOAA polar-orbiting satellite microwave data. *Mon. Wea. Rev.*, 119, 159-168.

Appendix 6.

Presented at the 19th Conf. Hurricanes and Tropical
Meteorology, Miami, Fl, May, 1991.

4A.4

The basic relationship between tropical cyclone intensity and the depth
of the environmental steering layer in the Australian region

Christopher S. Velden

Cooperative Institute for Meteorological Satellite Studies
University of Wisconsin-Madison
Madison, Wisconsin

Lance M. Leslie

Australian Bureau of Meteorology Research Centre
Melbourne, Victoria
Australia

1. INTRODUCTION

There is little question that the environmental flow accounts for a large fraction of tropical cyclone motion. Previous studies of the steering concept have suggested that tropical cyclone motion could best be approximated by either a mid-tropospheric level (500 or 700 mb), or a mass-weighted deep layer-mean (DLM) flow field such as the vertically-averaged wind over the 1000-100 mb layer. However, operational hurricane forecasters know from experience that, in general, weaker tropical cyclones move with a shallow lower-tropospheric flow while the more well-developed systems move with a deep-layer flow (Simpson 1971). The background on the development of environmental steering concepts is summarized in Elsberry *et al.* (1987).

The question pertaining to the optimum level, or layer, which best approximates tropical cyclone motion was quantitatively addressed by Dong and Neumann (1986). They found that the optimum depth of the deep layer for steering Atlantic hurricanes is greater than that for weaker tropical storms, and that deep layer steering is generally better than single-level steering (in agreement with Pike 1987). Chan and Gray (1982) examined cases from three tropical cyclone basins including the Australian region, in which they documented the deviations of storm motion from selected levels/layers of environmental steering. Deep-layer steering was found to be a good descriptor of cyclone movement. These studies suffered somewhat from generality in that only broad intensity classes (tropical storm and hurricane) were considered.

In this paper we expand on this general approach in an attempt to specifically identify the relationship between tropical cyclone intensity and barotropic motion in the Australian region tropical cyclone basin. The physical reasoning behind this suspected relationship is based on the hypothesis that an increase in intensity is generally associated with greater vertical development of the cyclonic vortex, which in turn is advected by an environmental flow of greater depth. A proper and detailed identification of the optimum steering layer will not only be useful for subjective predictions by operational forecasters, but can provide improved initial analysis input for statistical and barotropic track forecast models which initialize on layer-mean wind analyses (such as the operational barotropic model employed in Australia

which uses a 1000-100 mb deep layer-mean). These findings should also contribute to further studies of the environmental influences on tropical cyclone motion in the Australian region, through more proper identification of the basic flow.

A nondivergent barotropic model is employed in this study to investigate the effects on track forecast errors by varying the vertical extent of the initial wind analyses (environmental steering flow) based on current storm intensity. The results will allow for an assessment of the importance of the initial analysis and intensity information in barotropic track forecasting.

2. DATA SAMPLE

Tropical cyclone "best track" data from Australian region storms are on archive at the Australian Bureau of Meteorology. This data set consists of 6-h information that includes the storm date/time, and observations/estimates of current position, central pressure, speed and direction. Also on archive are the objective, operational mandatory-level wind analyses over the Australian region for the period 1971 to the present (Mills and Seaman 1990). Input to the nondivergent barotropic track-forecast model utilized in this study (discussed in the next section) is provided from a selection of these individual mandatory-level wind analyses, and mass-weighted layer-means derived from these horizontal analyses (Pike 1985). The selection process was based on subjective reasoning and previous studies (e.g. Dong and Neumann 1986; Pike 1987).

For the present study, 300 cases from 1971-1990 over the Australian region tropical cyclone basin (roughly 0-40 S and 100-170 E; see Fig. 1) were selected that cover a wide, but evenly-distributed range of intensities from depressions to very strong cyclones. The selection process only required each case to have 48 hours of subsequent storm track for model forecast verification, and a 24-h separation between cases to help minimize serial correlations. The Australian region basin offers a severe test of environmental steering concepts since it is characterized by relatively strong vertical shear zones, early track recurvatures and poleward movement, and frequent continental influences (Peak and Elsberry 1984). These effects quite often result in nonpersistent, nonclimatological tracks (Holland 1984) and difficult forecasts (Pike and Neumann 1987).

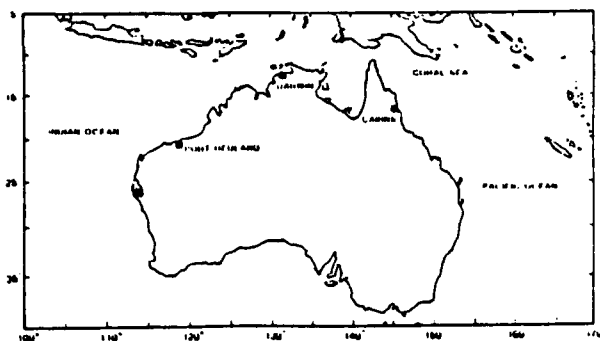


Figure 1. Australian region tropical cyclone domain.

3. FORECAST MODEL

The procedures for analyzing the wind field and predicting the forecast track are: 1) the removal of the tropical cyclone vortex from the initial wind analysis and replacement with the environmental flow; 2) a nondivergent barotropic forecast of the environmental flow field; and 3) a point (storm center) trajectory forecast based on the barotropic forecast of the environmental flow. This methodology was chosen to minimize the effects on the tropical cyclone motion due to the vortex specification and interaction, and to focus specifically on the effects of varying the environmental flow field.

The axisymmetric tropical cyclone vortex is removed from the initial objective wind analysis by zeroing out all gridpoint values within a specified radius of the storm center. This radius is determined from the operationally-analyzed outermost closed isobar. Bi-linear interpolation from surrounding gridpoint values just outside the specified radius is used to re-assign values to all gridpoints that were zeroed out. This simple procedure, in effect, approximates the environmental flow over the original vortex region.

The environmental flow is assumed to be governed by the nondivergent barotropic vorticity equation, which expresses conservation of the vertical component of absolute vorticity following parcels on a sphere. The model equations are solved using leapfrog time differencing and centered spatial differencing on a limited-area, latitude-longitude grid located over the Australian region analysis domain (Fig. 1). The latitude and longitude increments are equal and fixed at one degree. Since the model domain is confined to lower latitudes, numerical problems with this finite-difference scheme at higher latitudes (e.g., convergence of the meridians, singularities at the poles) do not arise. The solution procedure is as follows: the vorticity field is calculated from the initial streamfunction field, then the forcing term is computed and the Helmholtz equation is solved for Z_w/Z_t . Finally, the streamfunction is updated in time.

The final step is a simple trajectory procedure which follows a point (storm center) in the fluid (environmental flow) during the barotropic model integration (Velden et al. 1984). This step is necessary because of the elimination

of the vortex (and associated vorticity center) as described above. The trajectory begins at the specified storm center location, and is calculated after each time step based on the barotropic forecast of the environmental flow.

This forecast procedure is both simple and economical, and has been employed in previous sensitivity/impact studies (Velden et al. 1984; Velden 1990). It is appropriate for use in our analysis as it provides for a forecast based purely on the specified environmental steering current. The results presented in the next section are based upon forecasts from this model.

4. RESULTS

We first consider the relative performance of selected single-level wind analyses (mandatory levels), single-level combinations (with individual levels given weights determined by regression equations provided by the ERL-Hurricane Research Division), and vertically averaged (mass-weighted) tropospheric layer-means as input to the model for the entire sample, before stratifying by storm intensity. Mean forecast errors (MFE) for the 300 cases are shown in Table 1. Care must be taken in the interpretation of this table. As we will show later in the text, storms with different intensities move with different flow regimes and inherent forecast difficulty levels. Since we deliberately chose a sample with an evenly-distributed range of intensities, and not a climatological intensity distribution, generalizations about Australian region tropical cyclone steering cannot be gleaned from this particular table. The focus is on the relative differences between the MFE for a sample with evenly-distributed intensities.

Table 1 shows 12, 24, 36 and 48-h forecasts (km) from the barotropic model initialized with selected wind analyses. Considering first the single-level analyses, the results show that the MFE for 700 mb is slightly lower than 850 mb, moderately lower than 500 mb and significantly lower (student-t test 95 % significance level will be used throughout the paper) than the 400 mb MFE. The MFE from the selected single-level combinations are generally higher than the single-level MFE, which suggests that adding upper-tropospheric (outflow region) information is detrimental to approximating the steering current, at least in the context of barotropic track forecasting.

A substantial reduction in MFE occurs when layer-mean fields are used as input to the model. Overall, the 850-300 and 850-400 mb layer-means yield the lowest MFE, and are significantly lower than the MFE from the optimum single-level (700 mb) and the 1000-100 mb DLM commonly utilized in operational models that incorporate layer-mean wind analyses as input. This supports the findings of previous studies (e.g. Dong and Neumann, 1986; Pike 1987) that tropospheric layer-means, as opposed to single-levels, should be used to best approximate environmental steering. However, at least in the Australian region, the traditional 1000-100 mb DLM is not the optimal layer. This supports our previous observation and the contention by Holland (1984) that boundary and outflow layer asymmetries do not contribute to the basic current, and may even introduce variance, at least in the context of barotropic environmental steering. Holland (1984) also suggests the general

use of the 850-300 mb layer for approximating the basic current in Australian tropical cyclones. As discussed later, this layer is valid for intense systems, but is not optimum for weaker storms.

Table 1. Mean track forecast errors (km) from various wind analyses used to initialize the barotropic track forecast model. The number of cases is 100. The lowest MFE for each period is underlined.

Forecast interval (hrs)	12	24	36	48
<u>Single levels (mb)</u>				
850	108	211	280	381
700	106	209	272	375
500	111	216	286	389
400	117	226	297	415
<u>Single-level combinations (mb)</u>				
850,200	125	239	311	437
850,500,200	117	221	293	412
850,400,200	118	228	305	427
<u>Layer-means (mb)</u>				
1000-100	93	193	267	359
850-200	89	189	249	346
850-300	<u>85</u>	183	242	338
850-400	87	<u>182</u>	<u>240</u>	338
850-500	89	186	246	341
700-400	94	197	251	351
700-500	96	202	254	356

Given the results shown in Table 1, only the layer-mean fields are examined further. The MFE differences between the "best" three or four layer-means are quite small, and an optimal layer-mean is not obvious. This is especially true given the evidence presented later in the text that intense storms (in which the 850-300 mb layer-mean is optimum) exhibit a lower overall MFE than weaker storms. It is emphasized that these results should not be interpreted as a general finding for the Australian region basin, since our sample intensities are intentionally evenly-distributed, and not based on climatology.

To investigate the influence of tropical cyclone intensity (defined as the current minimum sea level pressure, MSLP) on the selection of the optimum steering layer, the sample is stratified into 10 mb intensity classes shown in Table 2 (while only the 48-h MFE are shown, similar results were found at other forecast intervals). From Table 2, our objective results seem to confirm intuitive reasoning that the motion of weaker storms is best approximated by shallow layer-means, and intense storms by deep layer-means. Figure 2 graphically represents the relationship between the optimum steering layer (lowest MFE) and intensity. It is clear a general relationship exists, although due to the somewhat narrow intensity stratification, the differences in MFE in Table 2 are generally not significant. This may, in part, be due to the variance in the best track intensity estimates that were derived almost solely from satellite techniques that were evolving during the period of this study (Holland 1981).

Table 2. 48-h mean track forecast errors (km) from various layer-mean wind analyses used to initialize the barotropic track forecast model for specified tropical cyclone intensity classes. The total number of cases is 100, which are fairly evenly distributed among intensity classes. The lowest forecast error for each intensity class is underlined.

Intensity class (mb)	>1005	995-1005	985-995	975-985	965-975	955-965	945-955	935-945	<935
no. of cases	25	25	25	25	50	50	25	25	50
<u>Layer-means (mb)</u>									
1000-100	389	374	367	364	367	364	347	338	324
850-200	383	365	357	355	348	339	328	326	313
850-300	371	362	355	351	331	332	<u>310</u>	<u>304</u>	<u>302</u>
850-400	343	341	349	344	<u>322</u>	<u>316</u>	334	341	339
850-500	<u>322</u>	<u>321</u>	<u>322</u>	<u>327</u>	332	329	356	360	356
700-400	348	338	347	342	345	341	361	365	368
700-500	342	<u>321</u>	340	346	359	367	372	377	372

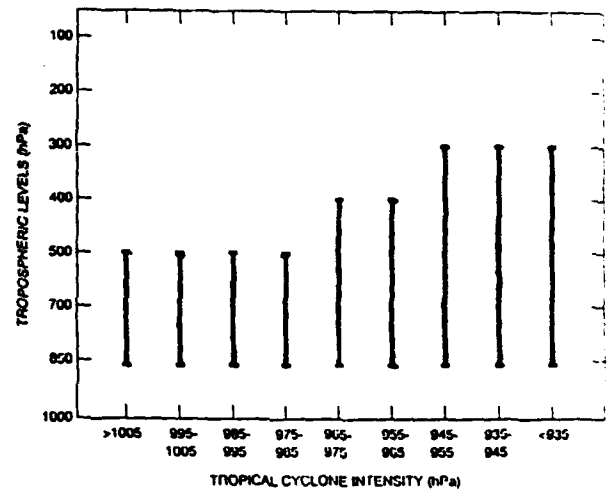


Figure 2. The relationship between tropical cyclone intensity (MSLP) and the depth of the steering layer in the Australian region. The thick bars indicate the layer-mean wind analysis that provides the optimum 48-h track forecast in each intensity category. (Note: as indicated in Table 2, there was a tie between the 850-500 and 700-500 mb layer-means for the 995-1005 mb intensity category).

It is suggested from Fig. 2 that a re-stratification into 3 broader intensity classes (> 975, 955-975, < 955 mb) would adequately represent the steering-intensity relationship. This broader intensity stratification will also reduce the likelihood of variance due to unrepresentative intensity estimates. The MFE (h) are presented in Table 3, and show that the 850-500 mb layer is optimal for the storms with intensities higher than 975 mb; the 850-400 mb layer is optimal for storms with intensities between 955 and 975 mb; and the 850-300 mb layer is optimal for storms with intensities lower than 955 mb. (Note: the 850-200 mb layer provided the lowest MFE for storms with intensities lower than 925 mb, however the very small number of cases prevented this result from being significant, is not shown).

Table 3. As in Table 2, except for different intensity classes.

Intensity class (mb)	> 975	955-975	< 955
no. of cases	100	100	100
Layer-means (mb)			
1000-100	374	365	336
850-200	365	344	322
850-300	360	332	203
850-400	345	318	338
850-500	333	330	357
700-400	344	343	365
700-500	340	356	374

Differences in the MFE between the layer with the lowest and next lowest values are significant for each intensity category. Table 4 presents a summary of the variability of these results. Shown for each layer-mean are the number of forecasts that yielded the best (and worst) 48-h position errors relative to the other layer-means, for each intensity category. The highest number of optimal forecasts in each intensity category corresponds to the layer-mean with the lowest MFE shown in Table 3, suggesting a strong degree of consistency in the results.

Similar results are also found with the 12, 24 and 36-h MFE (not shown), and specifically identify the greater depth of the optimal deep-layer environmental steering relative to increasing tropical cyclone intensity in the Australian region. This information should be very useful to operational forecasters for subjective purposes, and can be employed to more appropriately initialize operational statistical and barotropic numerical track forecast models.

It is interesting to note from Table 3 that the optimum layer MFE for the intense storms (< 955 mb) is significantly lower than the optimum layer MFE for the weaker storms (> 975 mb). This finding is consistent with the results of Dong and Neumann (1986) for easterly moving Atlantic hurricanes versus tropical storms. This could be physically related to the more persistent nature of deep-layer steering associated with the more

Table 4. A summary of the variability of the results in Table 3. The numbers indicate how many times each particular layer-mean yielded the best (worst) forecast for each intensity category.

Intensity class (mb)	> 975	955-975	< 955
no. of cases	100	100	100
Layer-means (mb)			
1000-100	6 (32)	8 (16)	16 (8)
850-200	5 (27)	10 (8)	23 (5)
850-300	6 (17)	20 (9)	34 (2)
850-400	21 (8)	31 (4)	17 (12)
850-500	16 (4)	13 (11)	3 (24)
700-400	12 (7)	14 (20)	4 (22)
700-500	14 (5)	4 (32)	3 (27)

intense storms, but could also be attributed to increased initial positioning errors associated with weaker systems (DeMaria et al. 1990).

The overall MFE when the optimal layer (based on the 3 intensity categories) is used in each individual case (dependent sample) to initialize the model is shown in Table 5. This method results in a significant reduction in MFE (up to 12% at 48 hours) over that of a fixed-layer (1000-100 mb) initialization that does not include intensity information (i.e. the current operational procedure at the Bureau of Meteorology in Australia). This is quite a remarkable improvement given the experiment involves only a modest change in the initial analyses provided to the forecast model.

While relative comparisons are the main focus of this paper, the forecast results using the optimal layer are also compared in an absolute sense to persistence and the official track forecasts from these 300 cases to assess the competitiveness of this numerical guidance (Table 5). It is shown that the MFE are much lower than persistence, and quite competitive with the official forecasts (derived from operational storm positions). This is despite the fact that the model is governed solely by environmental steering, and does not include the contributions to motion from linear and nonlinear effects of vortex propagation.

It has been shown that current intensity information is important in determining the optimum steering layer to initialize the track forecast model. It stands to reason that knowledge of the intensity tendency during the forecast period might also contribute to lowering of the forecast errors. Based on our findings above (Table 3), if the intensity jumps to a different class during the 48-h forecast, then the optimum layer-mean will change as well. Providing this information to the model should lower forecast errors relative to the assumption of a steady-state optimum layer-mean through the entire forecast period.

To investigate this, model forecasts were made on a 97 case sub-sample, with all cases having at least one intensity class change in the 48 hours from the initial time. The control forecasts consist of initializing the model with the optimum layer-mean, with no future intensity information included, as was done above (i.e. the optimum layer-mean determined at the initial time, based on the initial intensity, remains fixed during the 48-h integration). The forecast

Table 5. A comparison of mean track forecast errors (km) by different methods for the homogeneous sample of 300 cases. From the barotropic model forecasts, the operational layer-mean is the 1000-100 mb DLM (fixed for all cases), and the optimum layer-mean (variable in each case) is based on the intensity stratification of Table 3. The official forecasts were made from operational initial positions and all others from best track positions.

Forecast interval (hrs)	12	24	36	48
Method				
Persistence	87	203	358	505
Official	96	201	280	382
Operational layer-mean	93	193	267	359
Optimum layer-mean	81	172	230	319

experiments consist of including future intensity information from best track, official forecasts, and an experimental intensity forecast scheme. The best track results will provide an estimate of the maximum impact possible, while the latter two methods will give an idea of what is practical and achievable given the current state of intensity forecasting.

The future intensity information is incorporated into the prediction scheme in the following way: the model is initialized with all three optimum layer-means as described in Table 3. Simultaneous integrations (parallel runs) of the large scale flow (barotropic) are performed, with the point trajectory forecast component only operating on the layer-mean field appropriate to the initial intensity class. When the intensity class changes during the forecast, the trajectory forecast switches to the corresponding optimum layer-mean field at that point, and the integration continues. This method, in effect, keeps the point (storm center) trajectory forecast on the optimum layer-mean throughout the integration. Of course, improvements in MFE will depend on the ability to accurately forecast future intensity.

The results of these experiments are presented in Table 6. It is shown that by using best track future intensity information, the MFE are lowered by an additional 8-12 % relative to the fixed optimum layer-mean. Using official forecasts of intensity, MFE are not significantly changed, reflecting the lack of skill by current operational methods. However, employing intensity forecasts from an experimental statistical (Markov Chain) scheme (Leslie et al. 1991), modest improvements in the MFE are found (3-6 %). It should be noted that these results apply only to cases with subsequent intensity class changes, and are not reflective of the impact on the entire 300 case sample, 2/3 of which were not characterized by intensity class (optimum layer-mean) changes.

Table 6. Mean track forecast errors (km) on a 97 case sample where the observed (best track) tropical cyclone intensity changed at least one class during the 48-h forecast. Each set of MFE are a result of the barotropic model run with different input data.

Forecast interval (hrs)	24	36	48
Method			
Operational (1000-100 mb) layer-mean with no future intensity data	195	277	364
Optimum layer-mean (from Table 3) with no future intensity data	184	253	337
Optimum layer-mean with best-track future intensity data	163	232	305
Optimum layer-mean with official forecast of future intensity	186	249	339
Optimum layer-mean with Markov Chain forecast of future intensity	177	242	326

5. DISCUSSION

The results show that the initialization of a barotropic tropical cyclone track forecast model with a variable-depth wind analysis that best approximates the environmental steering can significantly reduce the MFE relative to a "fixed-depth" analysis. The current operational scheme at the Australian Bureau of Meteorology utilizes a 1000-100 mb DLM in all forecast situations regardless of intensity, as does the operational SANBAR barotropic model (Sanders et al. 1975) in the Atlantic and eastern North Pacific basins. This study shows that the selection of the optimum wind analysis is dependent on storm intensity, with tropospheric layer-means outperforming single-level analyses. The model MFE for weaker systems (> 975 mb) are minimized using the 850-500 mb layer-mean, while the optimal wind analysis for very intense storms (< 955 mb) is the 850-300 mb layer-mean.

These findings for the Australian region support the intuitive concept that the depth of the environmental steering increases with tropical cyclone intensity. The fact that a strong relationship was found in this tropical cyclone basin, which is characterized by relatively weak environmental flow regimes and erratic tracks, suggests the basic concept would apply in other basins. In fact, Dong and Neumann (1986) found similar results in the Atlantic, although their stratifications and optimal layer-means differed somewhat.

There are physical and environmental factors which can affect the basic relationships and optimum steering layer-means. Some of these (storm latitude, intensity tendency, season, specific area of development, and environmental easterlies versus westerlies regimes) will be a subject of future work, and can be incorporated into the operational schemes. There are other situations that could lead to deviations from the above results in individual storm events. Initial analysis and intensity estimate uncertainties (Holland 1981), land effects (Holland 1984), strongly sheared environments (Chan and Gray 1982), or subtropical "hybrid" developments might require special considerations.

The tropical cyclone vortex was eliminated from the flow field in our study to isolate the effects on forecast motion exclusively by the environmental flow. Thus, we have not considered the potential effects of the variable-depth analyses on the component of tropical cyclone motion associated with vortex propagation (Chan and Williams 1987; Fiorino and Elsberry 1989). However, these findings may be important to studies of the interaction of the vortex with the environment by more accurately defining the basic flow.

From an operational standpoint, the performance of the barotropic track forecast model with the inclusion of the intensity information should boost the confidence Australian forecasts have in the ability of these simple models to

predict tropical cyclone tracks. There has been a tendency to overlook these models with the recent influx of sophisticated schemes and dynamic models. Certainly, the sheer simplicity of the model dynamics will explain much of the forecast position error in barotropic track forecasting. However, it is suggested from these results that a significant part of the forecast error can be attributed simply to the improper specification of the depth of the wind analysis used to initialize these models.

Preliminary results also suggest that intensity prediction could be important to barotropic track forecasting. When prognostic intensity information is incorporated into the barotropic track forecast model (to determine if the optimum layer changes during the 48-h integration), MFE's are reduced. While current operational intensity forecast methods show limited skill, a statistical scheme being tested at the Australian Bureau of Meteorology (Leslie et al. 1991) is showing promise.

6. REFERENCES

- Chan, J.C.-L., and W.M. Gray, 1982: Tropical cyclone movement and surrounding flow relationships. *Mon. Wea. Rev.*, **110**, 1354-1374.
- Chan, J.C.-L., and R.T. Williams, 1987: Analytical and numerical studies of the beta-effect in tropical cyclone motion. Part 1. Zero mean flow. *J. Atmos. Sci.*, **44**, 1257-1264.
- DeMaria, M., M.B. Lawrence, and J.T. Kroll, 1990: An error analysis of Atlantic tropical cyclone track guidance models. *Wea. Forecasting*, **5**, 47-61.
- Dong, K., and C.J. Neumann, 1986: The relationship between tropical cyclone motion and environmental geostrophic flows. *Mon. Wea. Rev.*, **114**, 115-122.
- Elsberry, R.L., W.M. Frank, G.J. Holland, J.D. Jarrell, and R.L. Southern, 1987: *A global view of tropical cyclones*. Copies available from R.L. Elsberry, Dept. of Meteorology, Naval Postgrad. School, Monterey, CA 93943.
- Florino, M., and R.L. Elsberry, 1989: Some aspects of vortex structure related to tropical cyclone motion. *J. Atmos. Sci.*, **46**, 975-990.
- Holland, G.J., 1981: On the quality of the Australian tropical cyclone data base. *Aust. Meteor. Mag.*, **29**, 169-181.
- Holland, G.J., 1984: Tropical cyclones in the Australian/Southwest Pacific region. *Aust. Meteor. Mag.*, **32**, 1-33.
- Leslie, L.M., G.D. Hess, G.J. Holland, and R.P. Morrison, 1991: Forecasting intensity changes in tropical cyclones using Markov chain techniques. Submitted to *Wea. Forecasting*.
- Mills, G.A., and R.S. Seaman, 1990: The BMRC regional data assimilation system. *Mon. Wea. Rev.*, **118**, 1211-1237.
- Peak, J.E., and R.L. Elsberry, 1984: Dynamical-statistical model forecasts of Southern Hemisphere tropical cyclones. *Mon. Wea. Rev.*, **112**, 717-724.
- Pike, A.C., 1985: Geopotential heights and thicknesses as predictors of Atlantic tropical cyclone motion and intensity. *Mon. Wea. Rev.*, **113**, 931-939.
- Pike, A.C., 1987: A comparison of wind components and geopotential heights as statistical predictors of tropical cyclone motion. Ext. Abst. 17th Conf. Hurr. and Trop. Meteor., Miami, FL, Amer. Meteor. Soc., Boston, MA, 101-103.
- Pike, A.C., and C.J. Neumann, 1987: The variation of track forecast difficulty among tropical cyclone basins. *Wea. Forecasting*, **2**, 237-241.
- Sanders, F., A.C. Pike, and J.P. Gaertner, 1975: A barotropic model for operational prediction of tracks of tropical storms. *J. Appl. Meteor.*, **14**, 265-280.
- Simpson, R.H., 1971: The decision process in hurricane forecasting. NOAA Tech. Memo. NWS SR-53, U.S. Dept. of Commerce, Washington DC, 20233.
- Velden, C.S., W.L. Smith, and M. Mayfield, 1984: Application of VAS and TOVS to tropical cyclones. *Bull. Amer. Meteor. Soc.*, **65**, 1059-1067.
- Velden, C.S., 1990: The impact of satellite-derived winds on hurricane analysis and track forecasting. Ext. Abst. 5th Conf. Satellite Meteor. and Ocean., London, England, Amer. Meteor. Soc., Boston, MA, 215-219.

Appendix 7.

Presented at the 5th Conf. Satellite Meteorology
London, England, September, 1991.

Western North Pacific Tropical Cyclone Intensity Estimation From NOAA Polar Orbiting Satellite Microwave Data

Christopher S. Velden
Robert T. Merrill

Cooperative Institute for Meteorological Satellite Studies
University of Wisconsin-Space Science and Engineering Center
Madison, Wisconsin

1. INTRODUCTION

The ability of satellite-borne passive microwave radiometers to delineate the upper-tropospheric warm core of tropical cyclones has been demonstrated in numerous case studies (Rozenkranz et al., 1978; Kidder 1979; Grody and Shen, 1982 and others). Velden (1989) presents a detailed qualitative description of North Atlantic cases, and expands upon previous work (Kidder 1979; Velden and Smith, 1983) in developing quantitative relationships between the satellite-observed upper-tropospheric thermal anomaly and reconnaissance measured surface intensity. Standard errors of estimate were found to be 8 mb and 13 kts for surface pressure and maximum wind speed estimates, respectively.

With the need for alternate techniques to monitor storm intensity due to the discontinuance of aircraft reconnaissance missions into western North Pacific tropical cyclones, it was natural to investigate the possible applications of the microwave data in this region. The research presented in this paper examines cases in which NOAA polar-orbiting satellite Microwave Sounding Unit (MSU) observations were obtained during 1980-1984 western North Pacific tropical cyclones.

Two methods for estimating typhoon intensity are presented, and both rely on the premise that the strength of the warm anomaly in the typhoon eye region is directly related to the surface pressure via hydrostatic balance. The first method is the same as was applied in the Atlantic by Velden (1989), which derives relationships by statistically correlating the magnitude of the satellite-observed upper-level warm core with surface intensity. The second method, which is still under development, uses a forward model of the relationship between the variable horizontal temperature structure of typhoons and the MSU antenna pattern in an attempt to explicitly account for the coarse radiometer resolution (relative to the typhoon eye). The performance of the two models on a homogeneous sample will be presented at the meeting.

2. DATA SAMPLE

Satellite overpasses of western North Pacific tropical cyclones from 1980 through 1984 were requested from the NOAA Satellite Data Services Division (SDSD) for cases where the tropical cyclone center was within 6 degrees longitude of the satellite subpoint, and an aircraft reconnaissance observation was available near the time of the overpass. A total of 82 cases covering a wide range of intensities satisfied the above criteria and constitute the data sample in this study.

Air Force reconnaissance center fixes and minimum sea level pressures (MSLP) have been compiled at Colorado State University and were made available to us. Surface pressure anomalies (ΔP_{sfc}) are determined by subtracting the MSLP from the environmental surface pressure, as determined from operational Western Pacific surface analyses on archive at the University of Wisconsin Department of Meteorology. Estimates of the maximum surface wind speed (V_{max}) are obtained from post-analyzed "best track" information. Where possible, the aircraft-observed eye diameter and the MSLP tendency from consecutive reconnaissance missions are recorded as ancillary data and examined for their influence on the statistical relationships. The eye diameter is also a critical input parameter to the physical model described in section 4.

3. STATISTICAL METHOD

This procedure involves determining the strength of the upper-tropospheric warm anomaly in the tropical cyclone center as observed in the satellite microwave data, and correlating it with the aircraft-observed MSLP and best track V_{max} . Warm anomaly strengths based on microwave-only soundings have been shown to be superior to those based on the raw MSU radiances (Velden et al. 1990). Soundings are produced interactively on the Man computer Interactive Data Access System (McIDAS, Suomi et al. 1983), using the physical iterative solution of Smith (1970) which takes advantage of all four microwave channels available and contains built-in precipitation attenuation checks. Most of the microwave radiance information provided to the retrieval algorithm near the level of maximum warming in the tropical cyclone center (250 mb) is supplied by the 54.96 GHz channel (MSU channel 3). Some examples of the 54.96 GHz radiance signal over typhoons in imagery format is presented in Fig. 1. For each of the 82 cases, a microwave sounding is generated in the eye, and at 10 environmental locations surrounding the storm which are not affected by the core warming, typically at a 600-1000 km radius. The values of the 250 mb temperature at the 10 environmental locations are averaged, and this value is subtracted from the 250 mb temperature derived in the eye sounding. The resulting quantity (ΔT_{250}) is a measure of the tropical cyclone upper-level warm anomaly as depicted by the microwave data. A detailed description of the procedure may be found in Velden and Smith (1983).

Several classes of statistical models are derived, each using successively more ancillary information in an attempt to reduce the error of estimate. The basic relationships that are derived only require knowledge of the tropical cyclone

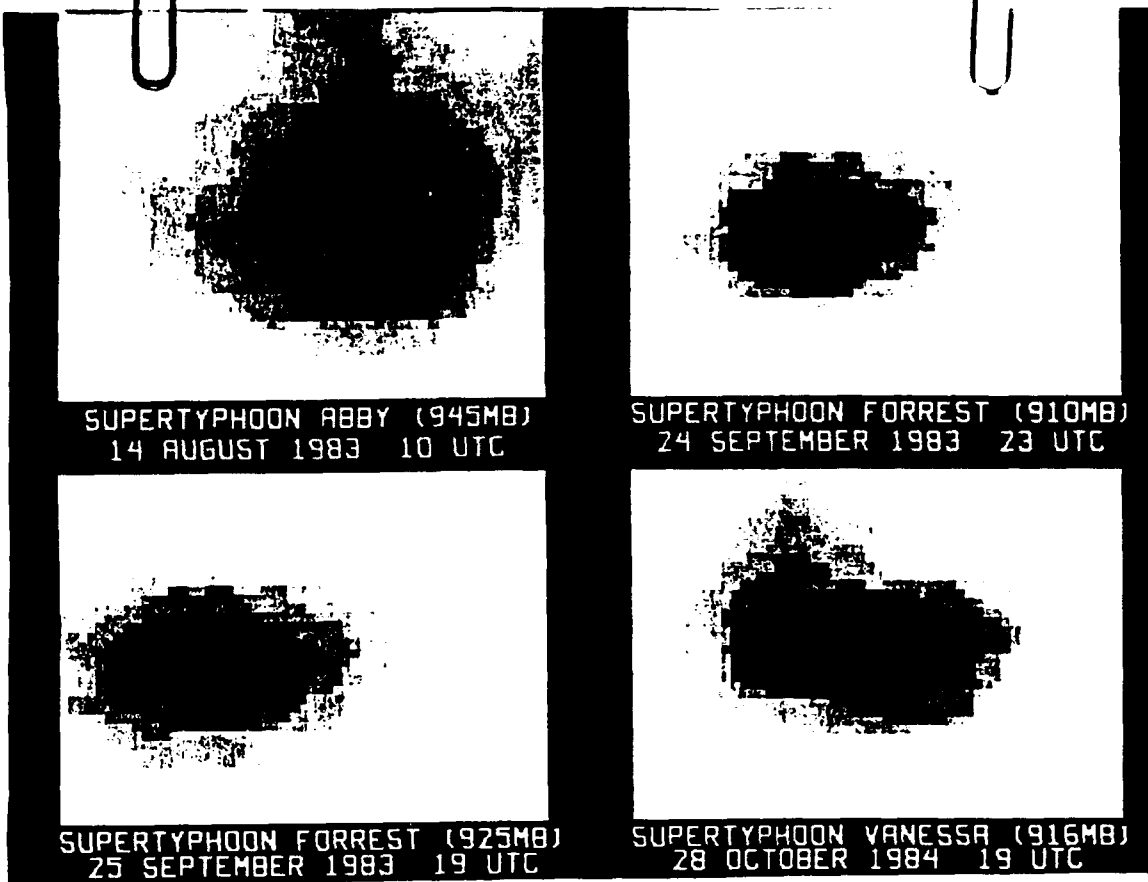


Fig. 1. Examples of NOAA satellite MSU 54.96 GHz imagery over selected western North Pacific super-typhoons. The warm cores are represented by the dark areas.

latitude and the satellite-derived ΔT_{250} , which are available for all 82 cases. The next class adds an eye diameter term (in this study determined by aircraft reconnaissance), which reduces the sample to 52 cases when an eye was observed. Finally, a further stratification is based on surface intensity tendency (also taken from reconnaissance reports), reducing the sample for this class to 44 cases. A sequence of statistical relationships beginning with a simple linear model (ΔT_{250} versus ΔP_{sfc} or V_{max}) is presented for each class.

3.1 Basic Relationships

We first consider the simplest regression models using all 82 cases. Figure 2 shows scatter plots of the relationship between the satellite-depicted ΔT_{250} and the surface parameters ΔP_{sfc} and V_{max} . The statistical model coefficients and errors of estimate for ΔT_{250} regressed against ΔP_{sfc} and V_{max} are given in Tables 1 and 2, respectively.

Considering the ΔP_{sfc} parameter, the simple linear model (sequence 1 in Table 1) yields a standard error of 14.1 mb. To allow for the apparent nonlinearity in the relationship beyond 5 degrees evident in Fig. 2, a stepwise multiple regression is used to select coefficients of a low order polynomial which are significant above the 95% confidence limit. A quadratic function of ΔT_{250} was found to yield the "best" fit (sequence 2). The additional term $(\Delta T_{250})^2$ has a minimal impact on low values of ΔT_{250} , but helps to reduce the intensity estimates for large values of ΔT_{250} .

As a result, the standard error is lowered by almost 1/2 mb with the inclusion of this term. A second nonlinear term ($\Delta T_{250} * LAT$) also provides statistically significant information to the model and reduces the error by .6 mb (sequence 3). The final model which includes all linear and nonlinear terms (sequence 4) results in an overall reduction of the standard error to 13.2 mb.

The 13.2 mb standard error does not necessarily reflect the accuracy that might be expected if the technique were to be used in a typical operational setting. Examination of our 82 case sample relative to climatology reveals that our sample is biased towards more intense storms. Since the stronger storms tend to lead to larger errors, the overall standard error of our sample (sequence 4) will also be biased high. To account for this, the model coefficients are re-derived by weighting the sample intensity distribution to be more representative of a climatological distribution from the period in which are cases were selected. The resulting model is given in sequence 5. The regression coefficients change very little from that in sequence 4, however, the standard error is 1.8 mb lower.

The regression models for V_{max} shown in Table 2 follow a similar development. The linear model yields a standard error of 17.3 kts, which is reduced to 15.4 kts when nonlinear terms are incorporated (sequence 4). The model standard error is reduced to 13.4 kts when an adjustment is made to remove the high intensity bias in our sample (sequence 5).

The slopes of the regression models are dependent upon how fully the actual eye warming is being resolved in the satellite radiances. The broader the horizontal extent of the maximum warming in the core region (typically 10-70 km), the more fully resolved it will be in the MSU observations (110 km hor. resolution at nadir). Given this concept, ancillary data that provides additional information about the size or structure of the warm core anomaly should improve upon the basic relationships, and this is examined next.

3.2 Effects of Including Eye Size

Reconnaissance reports of eye diameter were available in 52 of our 82 cases. Based on this sample, the regression models are re-derived with the inclusion of an eye size term. Adding an eye

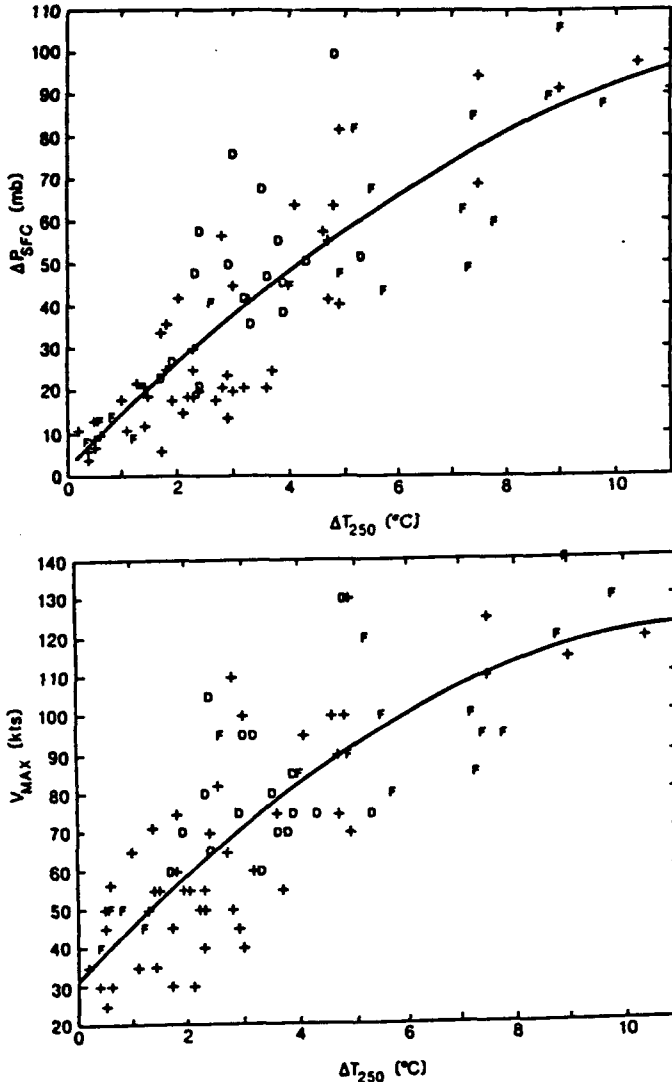


Fig. 2. a) Scatter plot showing the relationship between the 250 mb satellite-derived temperature anomaly (ΔT_{250}) and the reconnaissance-observed surface pressure anomaly (ΔP_{SFC}) in western North Pacific tropical cyclones. b) Same as a), except for ΔT_{250} versus V_{MAX} , where V_{MAX} is the maximum sustained winds from best track data. D's represent steady deepeners and F's represent steady fillers, discussed in the text.

Table 1. Coefficients and error characteristics for the relationship between ΔT_{250} and ΔP_{SFC} on the full 82 case sample. R^2 is the fraction of explained variance and SE is the standard error of estimate (mb). The sample average and SE for ΔP_{SFC} are 41 and 27 mb, respectively. The final relationship (sequence 5) is re-derived from an adjusted sample based on a climatological intensity distribution.

Sequence	Variable	Coefficient	R^2	SE
1	Constant	8.26		
	ΔT_{250}	9.18	.73	14.1
2	Constant	1.79		
	ΔT_{250}	13.28		
	$(\Delta T_{250})^2$	-.42	.75	13.7
3	Constant	6.31		
	ΔT_{250}	13.28		
	$\Delta T_{250} \cdot \text{LAT}$	-.16	.76	13.5
4	Constant	.16		
	ΔT_{250}	17.09		
	$(\Delta T_{250})^2$	-.41		
	$\Delta T_{250} \cdot \text{LAT}$	-.16	.76	13.2
5	Constant	-.51		
	ΔT_{250}	17.21		
	$(\Delta T_{250})^2$	-.42		
	$\Delta T_{250} \cdot \text{LAT}$	-.15	.81	11.4

Table 2. Coefficients and error characteristics for the relationship between ΔT_{250} and V_{MAX} on the full 82 case sample. R^2 is the fraction of explained variance and SE is the standard error of estimate (kts). The sample average and SE for V_{MAX} are 73 and 29 kts, respectively. The final relationship (sequence 5) is derived from an adjusted sample based on a climatological intensity distribution.

Sequence	Variable	Coefficient	R^2	SE
1	Constant	40.35		
	ΔT_{250}	9.23	.65	17.3
2	Constant	30.72		
	ΔT_{250}	15.32		
	$(\Delta T_{250})^2$	-.63	.67	16.7
3	Constant	37.65		
	ΔT_{250}	14.92		
	$\Delta T_{250} \cdot \text{LAT}$	-.23	.68	16.5
4	Constant	28.46		
	ΔT_{250}	20.61		
	$(\Delta T_{250})^2$	-.60		
	$\Delta T_{250} \cdot \text{LAT}$	-.22	.70	15.4
5	Constant	24.63		
	ΔT_{250}	21.30		
	$(\Delta T_{250})^2$	-.61		
	$\Delta T_{250} \cdot \text{LAT}$	-.21	.79	13.4

size term to the V_{max} model yields no significant improvement (95% level), and therefore its analysis is not shown. However, the addition of an eye size term to the ΔP_{sfc} model results in a standard error reduction of .6 mb (compare sequences 3 and 4 of Table 3), while adding 2% of explained variance. While the effects of the eye size term are small on this sample, it is shown below that this term adds important information in cases of steadily deepening tropical cyclones.

3.3 Effects of Stratification Based on Intensity Tendency

The regression models for the steadily filling storms (17 cases) are shown in Tables 4 and 5. The overall correlations are higher and the standard errors significantly reduced over that of the models which did not incorporate any past intensity information (Tables 1 and 2). This is not surprising since filling storms generally exhibit larger warm cores as discussed previously, and thus are more fully and consistently resolved by the MSU observations. These results are an indication that this intensity estimation method will work the best for this class of storms.

The regression models (ΔP_{sfc}) for the steadily deepening storms (17 cases) are shown in Table 6. (No statistically significant correlations were found for any of the ΔT_{250} versus V_{max} models). In general, the error characteristics are considerably larger than those associated with the filling systems. Only the linear and eye size terms, and no nonlinear terms, were found to be statistically significant contributors to the reduction of the standard error. This may in part be due to the sample distribution. All 17 cases fall within a ΔT_{250} range of 2-5 C, where the relationships show a linear tendency (Fig. 2). The sensitivity of the relationship to eye size in this class is very apparent, explaining an additional 21% of the variance (compare sequences 2 and 3).

Table 3. Coefficients and error characteristics for the relationship between ΔT_{250} and ΔP_{sfc} , including an eye size term (mb) on a 52 case sample. R^2 is the fraction of explained variance and SE is the standard error of estimate (mb). The sample average and SE for ΔP_{sfc} are 52 and 27 mb, respectively.

Sequence	Variable	Coefficient	R^2	SE
1	Constant	15.32		
	ΔT_{250}	8.50	.69	15.0
2	Constant	.54		
	ΔT_{250}	15.98		
	$(\Delta T_{250})^2$	-.68	.72	14.2
3	Constant	-1.93		
	ΔT_{250}	19.51		
	$(\Delta T_{250})^2$	-.69		
	$\Delta T_{250} \cdot \text{LAT}$	-.14	.73	13.8
4	Constant	5.69		
	ΔT_{250}	20.33		
	$(\Delta T_{250})^2$	-.71		
	$\Delta T_{250} \cdot \text{LAT}$	-.14		
	EYE	-.43	.75	13.2

Table 4. Coefficients and error characteristics for the relationship between ΔT_{250} and ΔP_{sfc} on a 17 case sample of steadily filling storms. R^2 is the fraction of explained variance and SE is the standard error of estimate (mb). The sample average and SE for ΔP_{sfc} are 53.7 and 30.7 mb, respectively.

Sequence	Variable	Coefficient	R^2	SE
1	Constant	7.83		
	ΔT_{250}	8.84	.80	13.6
2	Constant	8.88		
	ΔT_{250}	15.30		
	$\Delta T_{250} \cdot \text{LAT}$	-.27	.85	11.8
3	Constant	-4.38		
	ΔT_{250}	29.34		
	$(\Delta T_{250})^2$	-1.03		
	$\Delta T_{250} \cdot \text{LAT}$	-.64	.90	9.5

Table 5. Coefficients and error characteristics for the relationship between ΔT_{250} and V_{max} on a 17 case sample of steadily filling storms. R^2 is the fraction of explained variance and SE is the standard error of estimate (kts). The sample average and SE for V_{max} are 89.4 and 29.6 kts, respectively.

Sequence	Variable	Coefficient	R^2	SE
1	Constant	46.84		
	ΔT_{250}	8.21	.74	15.3
2	Constant	48.12		
	ΔT_{250}	16.36		
	$\Delta T_{250} \cdot \text{LAT}$	-.34	.83	12.3
3	Constant	30.69		
	ΔT_{250}	34.84		
	$(\Delta T_{250})^2$	-1.36		
	$\Delta T_{250} \cdot \text{LAT}$	-.57	.93	8.1

Table 6. Coefficients and error characteristics for the relationship between ΔT_{250} and ΔP_{sfc} on a 17 case sample of steadily deepening storms. Sequence 2 and 3 include the effects of adding an eye size term (mb) on a 14 case sub-sample. R^2 is the fraction of explained variance and SE is the standard error of estimate (mb). The 17 case sample average and SE for ΔP_{sfc} are 49 and 19 mb, respectively. The 14 case sample average and SE for ΔP_{sfc} are 31 and 19 mb, respectively.

Sequence	Variable	Coefficient	R^2	SE
1	Constant	14.55		
	ΔT_{250}	10.54	.24	17.0
2	Constant	17.39		
	ΔT_{250}	10.49	.23	17.6
3	Constant	31.64		
	ΔT_{250}	12.66		
	EYE	-.97	.44	15.1

4. PHYSICAL METHOD

The statistical methods described above have two limitations. First, as described in section 3.1, the coarse horizontal and vertical resolution of the microwave sounder results in an averaging across the region of peak warming (Fig. 3), such that the measured eye temperature is less than the actual temperature. The second limitation is that ground truth aircraft estimates are necessary to develop the relationships.

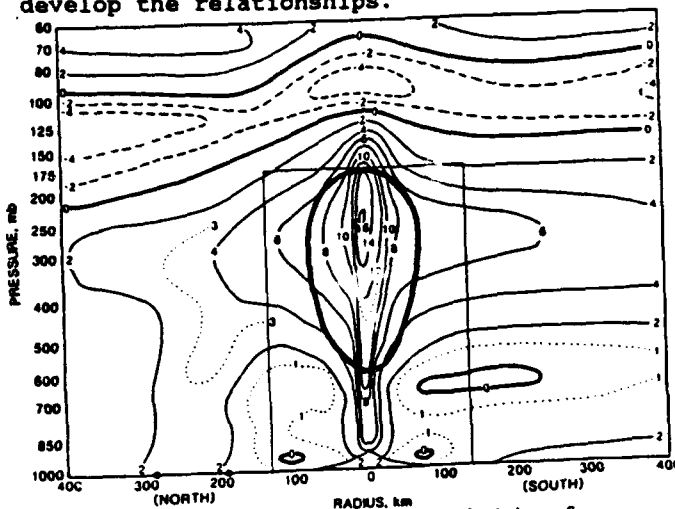


Fig. 3. Cross section in radius and height of temperature anomalies in Hurricane Inez (1966) based on rawinsondes (located at black dots on abscissa), aircraft flights in the low, middle, and upper troposphere (within rectangular outline, Hawkins and Imbembo 1976), and the mean hurricane stratospheric structure from Koteswaram (1967). Anomalies are relative to the mean annual sounding for the West Indies (Jordan 1958). If Inez were viewed at nadir and centered in the antenna footprint, roughly half of the energy received by MSU channel 3 would come from inside the oval marked by the heavy line.

The physical retrieval process can be divided into two parts; a horizontal structure retrieval (henceforth called simply "horizontal retrieval") and an eye sounding retrieval. The purpose of the horizontal retrieval is to extract the distribution of radiances which would be observed by a radiometer having perfect horizontal resolution from the measured raw (limb-corrected) radiances. The sought-after radiance distribution as a function of radius $R(r)$ is modeled as

$$R(r) = R_{env} + \Delta R \left[1 - \exp - \left(\frac{A}{r} \right)^b \right] \quad (1)$$

where R_{env} is the environmental radiance or brightness temperature, ΔR is the maximum (eye) radiance minus R_{env} , A is the horizontal scale of the warming, and b is a shape parameter. Holland (1980) fitted this function to surface pressure distributions, and it has since been applied to temperature profiles measured by aircraft at 180-240 mb (flights described in Shea and Gray 1973) and found to fit them acceptably, given suitable choices of R_{env} , ΔR , A , and b .

The horizontal retrieval is performed by inverting

$$R^{obs} = \int_{Area} R(x,y) F(x,y) dArea$$

using the nonlinear retrieval equation of Rodgers (1976)

$$X_{n+1} = X_0 + S_x K_n^T (K_n S_x K_n^T + S_0)^{-1} (R - R_n - K_n (X_0 - X_n))$$

where

X_{n+1} = $n+1$ estimate of structure parameters (R_{env} , ΔR , A , and b),

X_0 = background (constraint) values of structure parameters,

S_x = covariance of X_0 ,

R = observations,

S_0 = covariance of Y ,

R_n = n th estimate of observations from forward model operating on X_n ,

$$K_n = \left[\frac{\partial R_n}{\partial X_n} \right]$$

The background values X_0 and covariance matrix S_x were chosen based on application of (1) to the upper-tropospheric flight profiles mentioned above. Simulation of retrievals for these cases showed that better results were obtained if the aircraft observed eye radius and a reduced variance were used for A in place of the mean value for the entire sample.

ΔR can either be used directly to form a statistical relationship with ΔP_{sfc} , or an additional sounding retrieval step and hypsometric integration made to estimate ΔP_{sfc} directly. At present, we have only tested the horizontal retrieval portion on a small subset of the statistical model sample, and have not yet attempted the eye sounding retrieval.

A preliminary test of the horizontal retrieval concept has been made by selecting ten typhoon cases from the 82 case sample used to develop the statistical model. These cases were chosen to represent a range of intensities and intensity tendencies. Retrievals were made for each using several guess and covariance options. A single retrieval takes about 5 minutes on an IBM PS/2 Model 70. The results are evaluated by correlating the retrieved radiances (ΔR) and central pressure reductions ΔP_{sfc} , and comparing these correlations with those using the raw radiances (NR) and the $[\Delta T_{250}]$ and ΔP relationships found in the previous section. These comparisons are summarized in Table 7.

From these preliminary results we conclude that the physical method is slightly superior to a linear fit of the raw radiances (NR) and the statistical model $[\Delta T_{250}]$. Though the differences in explained variance between the experiments are not statistically significant for such a small sample, we conclude that the horizontal structure retrieval concept is practical and worthy of additional work.

Table 7. Summary of the relationships between raw (NR) and horizontally retrieved MSU-3 radiance anomalies (R1), vertically retrieved 250 mb temperature anomalies (T1) from lib-corrected MSU observations (ΔT_{250}), and sea level pressure anomaly (ΔP_{SLC}) for ten selected typhoon cases, 1980-84.

Parameter	Description of background structure	Predicted ΔP_{SLC}	
		Correlation	Std. Error
NR	Raw radiances (no horizontal retrieval)	0.697	21.1 mb
R1	Observed eye radius, non-zero covariances, anomaly from 1000 km radius value	0.820	16.9 mb
T1	ΔT_{250} from statistical model	0.757	19.3 mb
	Sample standard deviation		29.5 mb

5. DISCUSSION

Two methods are presented in this paper whereby estimates of western North Pacific tropical cyclone intensity can be made using microwave observations from NOAA polar orbiting satellites. The first method involves deriving statistical relationships between the satellite-depicted upper-tropospheric warm core anomaly and the observed surface intensity, and yields standard errors of around 13 mb and 15 kts for estimates of the surface pressure anomaly and maximum winds, respectively. These errors are reduced to approximately 11 mb and 13 kts when adjustments are made to the sample to more appropriately represent a typical western North Pacific tropical cyclone intensity distribution. Further reduction in errors result when ancillary data such as eye size and intensity tendency are incorporated into the regression models. Best results are achieved when the method is applied to filling storms, with the standard error of estimate of the surface pressure anomaly reduced to 9.5 mb. In deepening systems, the characteristic concentrated warm core is inconsistently resolved by the MSU observations, resulting in a much higher standard error.

The second method, still under development, attempts to account for variability in warm core structure by explicitly modeling the interaction between the warm core and the antenna pattern. A nonlinear retrieval method is used to solve for the environmental and core brightness temperature and the warm anomaly size and shape which produce model radiances which best match the observed ones. This method may be better able to cope with inter-storm and inter-basin variability, and is the only way in which intensity estimates from microwave sounders will be possible without ground truth from aircraft also being available.

6. REFERENCES

- Dvorak, F., 1975: Tropical cyclone intensity analysis and forecasting from satellite imagery. *Mon. Wea. Rev.*, **103**, 420-430.
- Grody, N., and W.C. Shen, 1982: Observations of Hurricane David (1979) using the microwave sounding unit. NOAA Tech. Rep. NESS 88, NESDIS, Washington, DC, 52 pp.
- Hawkins, H.F., and S.M. Imbenbo, 1976: The structure of small intense hurricane Inez 1966. *Mon. Wea. Rev.*, **104**, 418-442.
- Holland, G.J., 1980: An analytic model of the wind and pressure profiles in hurricanes. *Mon. Wea. Rev.*, **108**, 1212-1218.
- Jorden, C.L., 1958: Mean soundings for the West Indies area. *J. Meteor.*, **15**, 91-97.
- Kidder, S.Q., 1979: Determination of tropical cyclone central pressure and winds from satellite microwave data. Atmos. Sci. Paper No. 317, Col. St. Univ., Fort Collins, CO 80523.
- Koteswaram, P., 1967: On the structure of hurricanes in the upper troposphere and lower stratosphere. *Mon. Wea. Rev.*, **95**, 541-564.
- Martin, J., 1988: Tropical cyclone observation and forecasting with and without aircraft reconnaissance. Atmos. Sci. Paper. No. 428, Col. St. Univ., Fort Collins, CO 80523, 114 pp.
- Miller, B.I., 1964: A study of the filling of Hurricane Donna (1960) over land. *Mon. Wea. Rev.*, **92**, 389-406.
- Rodgers, C.D., 1976: Retrieval of atmospheric temperature and composition from remote measurements of thermal radiation. *Rev. Geophys. and Space Phys.*, **14**, 609-624.
- Rozenkranz, P.W., D.H. Staelin, and N.C. Grody, 1978: Typhoon June (1975) viewed by a scanning microwave spectrometer. *J. Geophys. Res.*, **83**, 1857-1868.
- Shea, D.J. and W.M. Gray, 1973: The hurricane's inner core region. I: Symmetric and asymmetric structure. *J. Atmos. Sci.*, **30**, 1544-1564.
- Smith, W.L., 1970: Iterative solution of the radiative transfer equation for temperature and absorbing gas profiles of an atmosphere. *Appl. Optics*, **9**, 1993-1999.
- Suomi, V.E., R. Fox, S.S. Limaye, and W.L. Smith, 1983: McIDAS III: A modern interactive data access and analysis system. *J. Clim. Appl. Meteor.*, **22**, 765-778.
- Velden, C.S., and W.L. Smith, 1983: Monitoring tropical cyclone evolution with NOAA satellite microwave observations. *J. Clim. Appl. Meteor.*, **22**, 714-724.
- Velden, C.S., 1989: Observational analyses of North Atlantic tropical cyclones from NOAA polar-orbiting satellite microwave data. *J. Appl. Meteor.*, **28**, 59-70.
- Velden, C.S., B.M. Goodman and R.T. Merrill, 1990: Western North Pacific tropical cyclone intensity estimation from NOAA polar-orbiting microwave data. Submitted to *Mon. Wea. Rev.*